Precise Control of District Heating Secondary Networks: A Dynamic Simulation Approach with Room Temperature Feedback

Anqing Wang[a] , Haichao Wang[a*], Tianyu Wang[a], Muyan Li[a], Zhiwen Luo[b], Risto Lahdelma[c,d]

[a] *Institute of Building Environment and Facility Engineering, Dalian University of Technology, Dalian 116024, China*

[b] *Welsh School of Architecture, Cardiff University, Cardiff, UK*

[c]*Department of Mathematics and Systems Analysis, Aalto University, School of Science, P.O. BOX 11100, Aalto, Finland*

d Department of Mechanical Engineering, Aalto University, P.O. BOX 14100, FI-00076, Aalto, Finland

Highlights

A novel hybrid control strategy integrating room temperature feedback is proposed.

A high-fidelity model coupling room dynamics with network hydraulics is developed.

±0.1°C thermal stability with 11.68% heat and 15.98% power savings is validated.

Abstract

As a critical infrastructure for building heating, district heating systems face the urgent dual challenge of decarburization and improving operational efficiency under increasingly dynamic demand.The traditional regulation of district heating systems is mainly based on the central control in heat plants and/or in the substations. However, the end-user control is becoming increasingly important in saving District Heating energy consumption. This study presents an integrated control strategy for district heating systems combining thermodynamic inlet temperature feedback regulation with an optimized heat exchange station supply temperature determination method. By synergistically coordinating these approaches with variable-frequency pump operation, the system achieves dual objectives of stabilizing end-user thermal comfort and reducing energy consumption. The research establishes a validated Modelica-based simulation model of a residential secondary heating network, benchmarked against operational field data. Implementation of PID-controlled inlet valves using room temperature feedback demonstrates precise thermal regulation capability, maintaining stable indoor conditions at 19±0.1°C. Comparative analysis reveals significant performance improvements, including 62.7-92.5% reduction in temperature standard deviation across monitored users and system-wide energy savings of 11.68% (thermal) and 15.98% (electrical). The proposed methodology shows substantial carbon reduction potential exceeding 2.16 $kgCO_2/m^2$ when scaled, offering a comprehensive solution for modernizing the control paradigms of district heating systems while addressing both hydraulic and thermodynamic optimization challenges.

Keywords: District heating system; Thermal inlet regulation; Hydraulic and thermodynamic balance; Room temperature control; Modelica simulation

Corresponding author at: Institute of Building Environment and Facility Engineering, Dalian University of Technology, Dalian 116024, China.

E-mail address: wanghaichao2002@163.com (H. Wang).

1 Introduction

Global energy use has doubled in the last four decades [1]. Buildings represent nearly 40% of total energy demand and contribute to a quarter of worldwide GHG emissions [2], with District Heating Systems (DHS) consuming approximately 40% of building energy [3]. During the period from 2004 to 2020, the energy consumption of DHS in China experienced a dramatic increase [4]. It is estimated that District Heating (DH) will expand to cover approximately 20 billion m² by 2030, inevitably resulting in significantly higher energy requirements [5]. In 2022, the CO_2 emissions from DHS reached 440 million tons, accounting for approximately 21% of the total emissions from buildings [6]. To address the challenges of global climate change, China pledged at the 75th United Nations General Assembly to strive for carbon peaking by 2030 and carbon neutrality by 2060, thereby promoting systematic carbon emission reductions while synergistically addressing ecological and environmental issues [7]. DHS often suffer from supply-demand mismatches due to inadequate integration of building thermal feedback in control strategies, leading to comfort compromises and energy inefficiencies. Thus, transforming DHS from a major carbon emitter into an efficient, flexible, and low-carbon energy infrastructure is not only necessary but urgent. Optimizing heat supply-demand coordination represents a critical opportunity to enhance both operational performance and environmental sustainability in modern DHS, directly contributing to the systemic emission reductions required for 2030 and 2060 targets.

DHS are pivotal for achieving building sector decarburization. The core challenge lies in precisely matching thermal supply with dynamic building demand to eliminate waste while ensuring comfort. The evolution of DHS control can be conceptualized as advancing from centralized, supply-side regulation toward distributed, demand-aware coordination. This review critically examines this progression, identifies persistent gaps at the building-network interface, and thereby positions the original contribution of this study.

China's DHS typically operate via centralized coordination between heat sources and substations [8][10]. This paradigm suffers from a “perception gap” due to the lack of real-time building thermal feedback integration, leading to supply-demand mismatches that compromise comfort and efficiency [7]. The primary barrier is the precision-cost tradeoff [11]. Even advanced studies that incorporate building feedback remain within this centralized paradigm. For instance, Li et al. [11][12] implemented predictive feedback control using effective room temperature to regulate substation valves, reducing temperature fluctuations and achieving 5.9%-7.9% energy savings. However, this approach is fundamentally categorized as DH centralized regulation and lacks integrated building-level control mechanisms. Similarly, while M.D et al. [13] integrated room and outdoor temperature for substation supply temperature control, it fails to address the regulation failure of terminal thermostatic valves caused by unstable hydraulic conditions [14][15]. This reveals a critical limitation: the absence of effective synergy between substation control and terminal devices in buildings.

The deployment of advanced sensor networks has catalyzed data-driven methods for thermal load forecasting. Machine learning techniques, such as Support Vector Regression (SVR) [16],

integrated black-box and physical models [17], and clustering-optimized Artificial Neural Network (ANN) [18], have achieved high prediction accuracy (Mean Absolute Percentage (MAPE) below 7.8%). However, the translation of these accurate predictions into precise room temperature control remains substantially limited [19]. The fundamental issue is the mismatch between the energy-balance basis of load forecasting and the nonlinear dynamics of room temperature, alongside the weak correlation between minor temperature fluctuations and system-level thermal loads. Merely relying on more accurate predictions cannot solve closed-loop control issues; it requires a deeper, embedded integration of predictive models with control strategies that account for building dynamics.

Hydraulic balance is crucial for equitable heat distribution [20][21]. However, even under balanced conditions, strong thermo-hydraulic coupling can lead to thermal imbalances [22]. Recent advanced methods, such as Model Predictive Control (MPC) combined with neural networks [23] and intelligent algorithm-based valve optimization [24], aim to address this. A persistent flaw in these studies is that buildings are either simplified as static load models (only suitable for hydraulic analysis) or, when dynamic room models are established, they are not deeply coupled with network-wide hydraulic dynamics in simulation. This reveals the second key limitation: hydraulic and thermal regulations remain decoupled in research, preventing true demand-supply matching.

Implementing distributed control on the secondary network side has become an important research direction. Currently, such studies primarily focus on regulating valves at individual branches or end units to achieve flow redistribution and hydraulic balance [25]. The core objective is to eliminate hydraulic imbalance and ensure the attainment of design or target flow rates. Many studies employ intelligent algorithms to optimize valve openings, aiming to minimize the hydraulic imbalance rate or bring branch flows closer to set values [25][26]. These methods can theoretically improve the spatial uniformity of heat distribution and have been shown to reduce overall system pumping energy consumption [27][28]. However, their control objectives and optimization variables consistently revolve around hydraulic parameters such as flow rate or pressure differential, failing to establish a closed-loop linkage with room temperature—the ultimate indicator of comfort and energy demand.

Research has shifted towards utilizing building thermal inertia for precise control[29][30]. Studies by Yuan et al. [31] and Hou et al. [32] employed thermal inertia data or MPC with room temperature as the core objective, achieving energy savings. Wang et al. [33] proposed an MPC-based zoned control for single buildings. However, these advanced building-side strategies are either confined to single buildings [33] with unverified feasibility for network coordination, or they merely function as advanced feedback signals for centralized set point optimization, failing to form a distributed synergistic closed-loop between building devices and network regulating equipment.

Existing research has identified several unresolved challenges in DHS system studies:

(1) Current studies treat hydraulic and thermal regulation as separate processes. Hydraulic adjustments focus on flow distribution but ignore building thermal dynamics, often leading to localized overheating or under heating and preventing true demand-supply matching.

(2) Mismatches between heat supply and user demand cause significant indoor temperature swings and energy waste. Without precise demand forecasting and dynamic control, thermal supply fails to align spatiotemporally with actual needs.

(3) Most DHS control remains centralized at heating stations, with limited exploration of building-side strategies, neglecting distributed optimization at end-user terminals.

To address these challenges, this study proposes the following solutions:

(1) Develops a full-scale secondary network simulation by coupling radiators with RC-based room models to enhance dynamic accuracy.

(2) Quantifies room temperature distribution under hydraulic balance, enabling comparative analysis of hydraulic and thermal equilibrium.

(3) Proposes a new method for setting heat station supply temperature and a hybrid DHS control strategy. By incorporating thermodynamic inlet temperature feedback, it reduces indoor temperature fluctuations, improves thermal comfort, and lowers station energy consumption.

2 Main contribution and novelty

This section introduces the three different control strategies and key innovations.

2.1 Control strategies

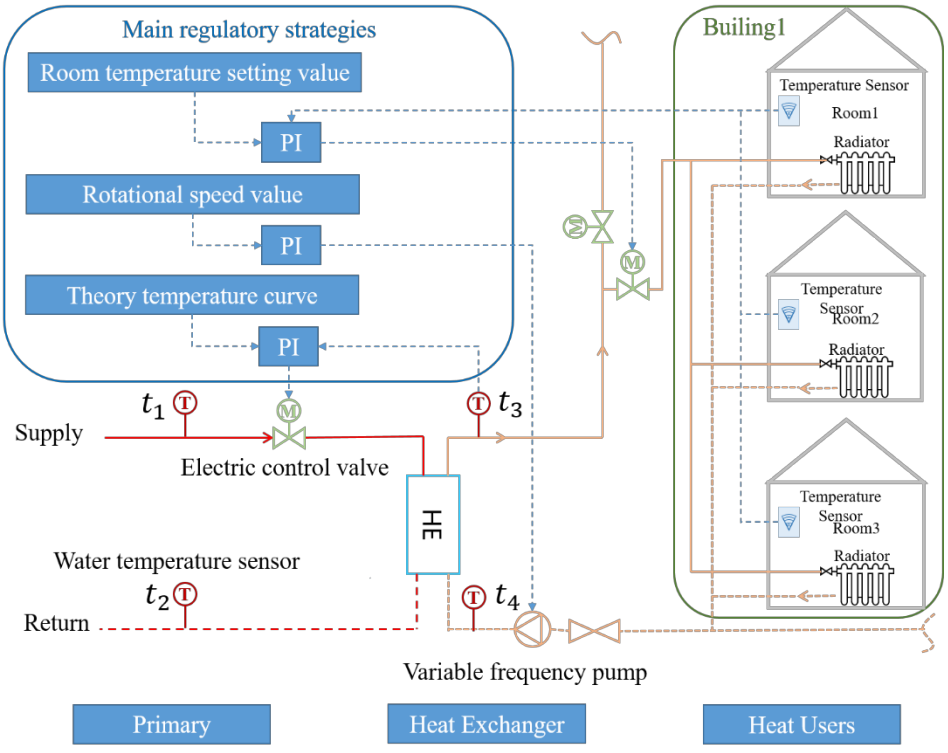

Fig 1. Centralized and distributed control of secondary networks

The control sequence of the DH substation, as schematically represented in Fig 1, operates through a hierarchical regulation framework: (i) primary side electric control valve governs heat

exchanger thermal output to maintain secondary side supply water temperature at set point , while (ii) secondary side flow rates are coordinately modulated through integrated variable frequency pump operation and thermal entrance control valve adjustments. The primary-side control strategy is not the focus of this study, but rather a means to maintain the dynamic set point of the secondary-side water supply temperature.

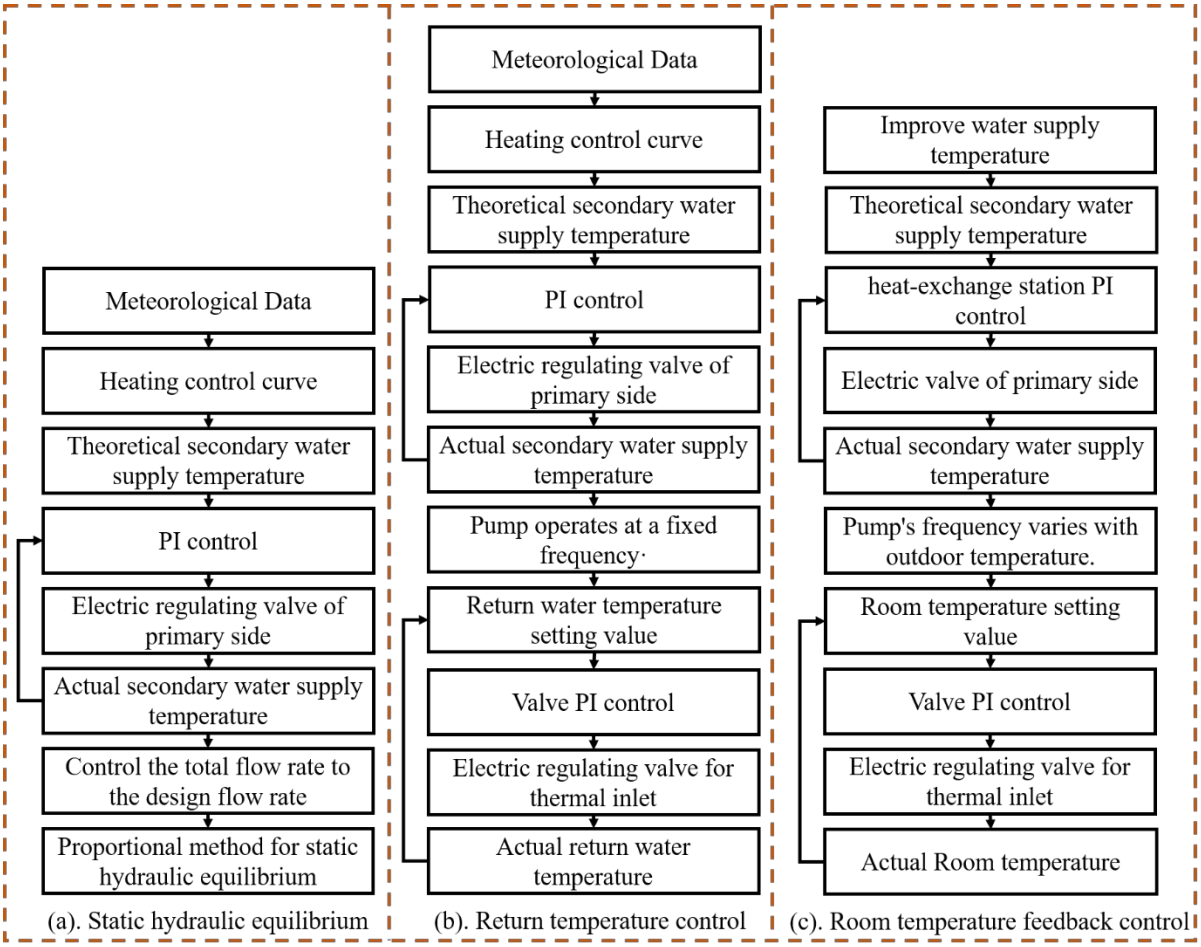

Fig 2. Control strategy for this study

This study utilizes a developed simulation model to evaluate two widely-adopted regulation strategies in district heating systems: Static hydraulic equilibrium(SHE) and Return water temperature control(RTC), which serve as benchmark cases for comparative analysis. Building upon this foundation, we propose an innovative methodology for determining optimal supply water temperature values at heat exchange substations. This approach is integrated with a closed-loop feedback mechanism utilizing Room temperature feedback control(RTFC) building thermal interfaces, thereby enabling enhanced precision in the operational control of secondary heating networks. The control principle of three methods are depicted in Fig 2.

According to Fig 2, in general, the primary-side valve ensures that the secondary-side supply water temperature reaches the target value, while the pump operates at either constant or variable flow rates. The end-user valves are regulated according to different strategies. In the SHE strategy, the total flow rate and end-user flow rates are maintained at their design values, valves and pumps on

the secondary side remain unadjusted, while the primary-side valve is regulated to ensure that the secondary supply water temperature matches the value on the target curve. In the RFC strategy, the supply water temperature is kept consistent with that in SHE, and the pump operates at a fixed frequency, the end-user valves are adjusted to maintain the return water temperature at the value specified by the target curve. In the RTFC strategy, end-user valves are directly regulated with a fixed indoor temperature as the target, and the target curve for supply water temperature is optimized accordingly, the water pump operates at variable frequency according to the temperature in different sections. The supply and return water temperature curves for both SHE and RFC are determined based on outdoor meteorological parameters.

Under the SHE strategy, maintaining consumer flow rates at design values ensures basic thermal demand fulfillment while keeping room temperature variations within an acceptable range (±1.5°C typically). In contrast, RTC indirectly regulates system flow distribution through uniform return temperature adjustment, conventionally employing fixed-speed pump operation. Crucially, both SHE and RTC operate as open-loop control architectures from the consumer perspective, lacking real-time responsiveness to building thermal dynamics. The RTFC paradigm fundamentally transforms this approach by establishing direct room temperature as the closed-loop control target, thereby achieving a strategic shift from "supply-oriented" to "demand-driven" regulation in district heating systems.

In practical cases, the temperature and flow rate on the primary side are adjusted to maintain the set supply water temperature on the secondary side. The supply water temperature and flow rate on the secondary side are regulated by engineers based on experience and user feedback. During a specific stage, the flow rate on the secondary side remains essentially unchanged, and the opening of the heat inlet valve remains constant during the heating period. Actually, the actual operation is similar with the SHE. The operation condition is depicted in Fig 3.

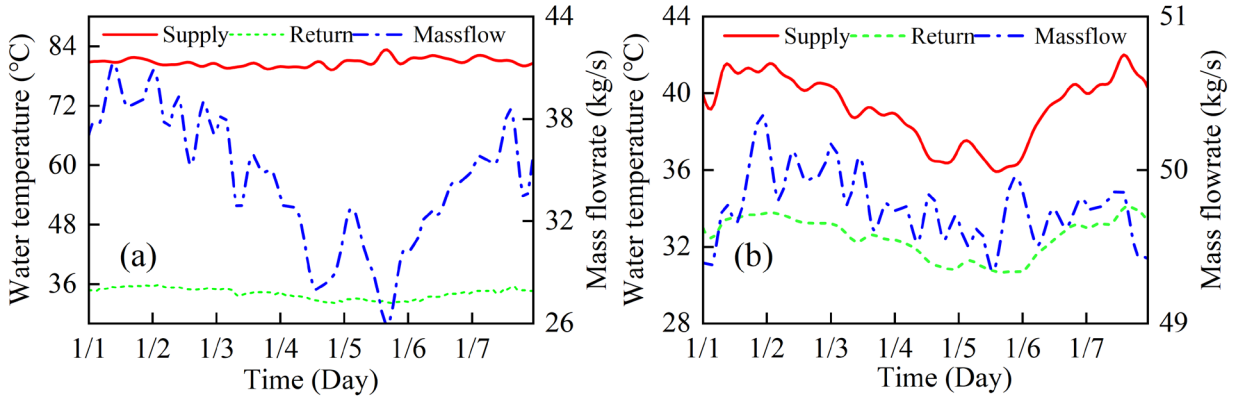

Fig 3. The actual operation, (a) Primary side, (b) Second side

2.2 Key innovations

This study investigates DHS regulation through a case study, demonstrating three key advancements:

(1) Establishment of a full-scale secondary network model integrating improved heat exchange

parameters and variable-speed pump operation;

(2) Implementation of thermal inlet feedback control achieving ±0.1K room temperature stability;

(3) Multi-level model validation including:

(i) pipe flow hydraulics via discretized differential equations,

(ii) RC-network building thermal modeling using energy balance principles,

(iii) measurement-calibrated valve model. The validation framework rigorously verifies both RC model accuracy and system-level hydraulic-thermal and pump energy performance.

3 Materials and Methods

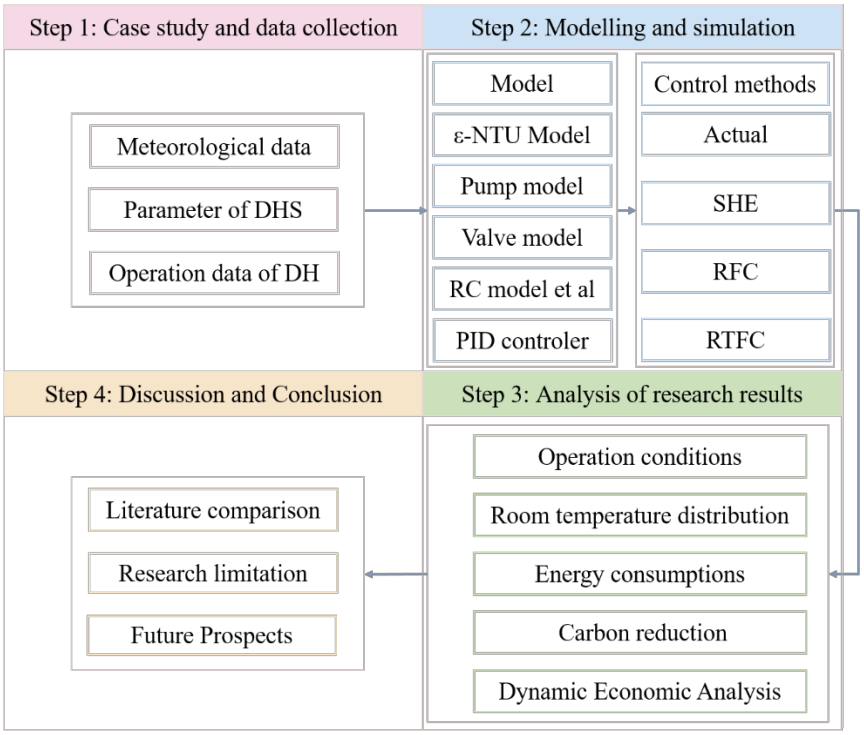

Fig 4. Research flowchart

The research flowchart of this study is shown in Fig 4. This study develops a high-fidelity DHS model by integrating DH case with OpenModelica simulations. The framework incorporates: (i) An energy-conservation-based RC network model that comprehensively resolves building thermal inertia through heat storage dynamics in building envelopes (interior walls, roofs, floors) and their convective coupling with indoor air, and (ii) Hydraulic model employing pipe flow differential equations to determine system characteristics without empirical resistance assumptions, while rigorously accounting for thermal losses during fluid distribution. This integrated approach provides both theoretical foundations and practical case validation for achieving precise temperature control and operational efficiency improvements in modern DHS. Tab 1 summarize three control strategies.

Tab 1. Table of three control strategies comparison

Methods/Control strategy	SHE	RTC	RTFC
Control objective	Set point of mass flowrate of pump and end-user	Dynamic set point of return water temperature	Set point of room temperature (19℃)
Pump control	PI for constant mass flowrate	Constant frequency	Variable frequency by outdoor temperature
Thermal inlet valve control	Constant opening	PI controller	PI controller
Primary side valve control	PI controller	PI controller	PI controller
Hydraulic conditions	Static (constant flow)	Variable mass flowrate	Variable mass flowrate

3.1 Case information

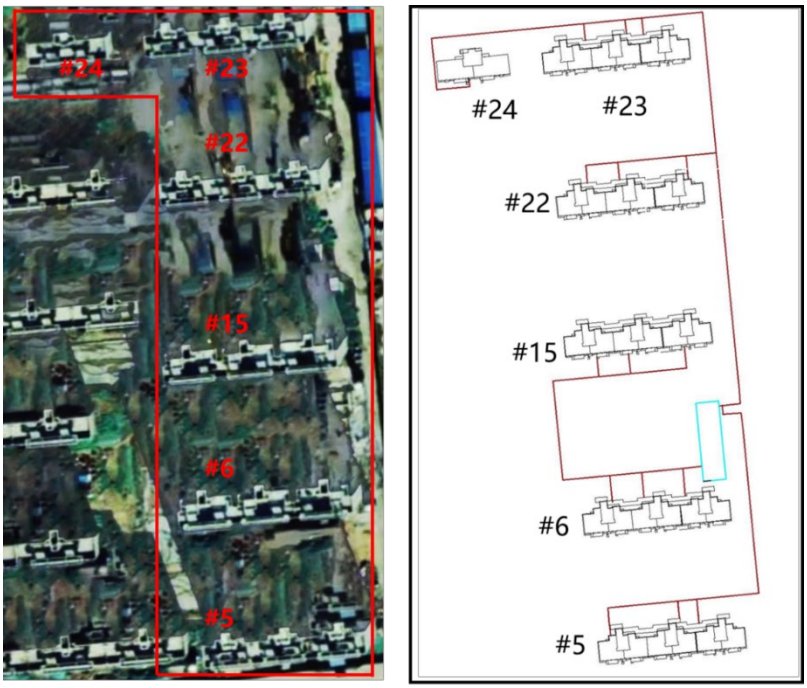

(a) (b)

Fig 5. The layout of heating pipeline network, (a) Satellite image, (b) design drawing

Fig 6. Floor plan of the studied space heating building, (a) Building Type I(#24), (b) Building type II(others)

This case study investigates a DHS in HuangHua City, CangZhou, Hebei Province, where a monitoring-equipped heat exchange station collects primary and secondary side parameters, including supply/return water temperature, pressure, flow rate and heat use at 10-minute intervals. The system serves six terminal buildings with two-household-per-floor layouts, comprising one Type I building (#24) with single thermal entry and five Type II buildings with triple thermal entries, forming 16 thermal user units that provide a complete experimental platform and reliable dataset for heating regulation strategy research. Type I has a base area of 683 m² with 8 floors, and Type II has a base area of 320 m² with 8 floors.The layout of the outdoor pipe network is shown in the Fig 5, the floor plan of two types buildings is shown in the Fig 6, and we have collected the local meteorological data as shown in the Fig 7, this is used for RC model simulating .

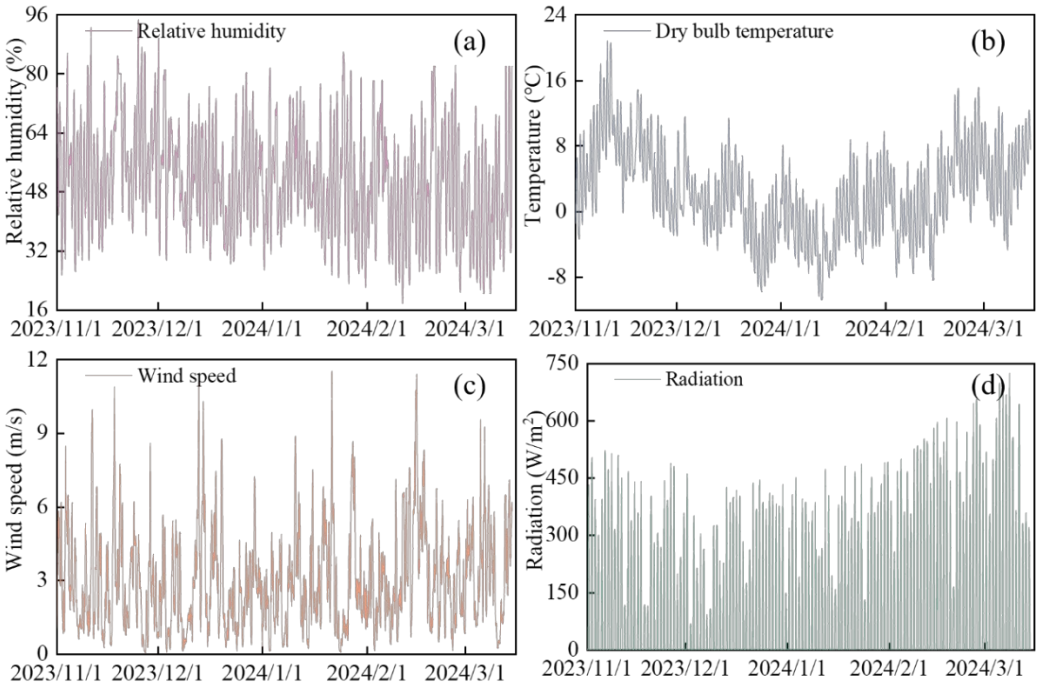

Fig 7. Meteorological parameters. (a) Relative humidity, (b) Dry bulb temperature, (c) Wind speed, (d) Radiation

3.2 Model Description

The models involved in this study include heat exchangers, water pumps, pipelines, valves, and buildings. Models from the Modelica Association library were used, and we developed an RC building room-temperature model. Combined with thermal inlet room temperature feedback control, the goal is to ensure room temperature stability and reduce energy consumption.

3.2.1 ε − NTU Model

The heat exchanger in the heat exchange station plays the role of a heat source in the secondary network. In the study, the counter flow ε − NTU model was used, and the specific mathematical principle is as follows, the key parameters of heat exchanger are shown in Tab 2.

$$Q_{max} = (Mc)_{min}(t_1' - t_2') \tag{1}$$

$$Q = Q_{max} \cdot \varepsilon \tag{2}$$

$$\varepsilon = \frac{1-\exp[-\frac{UA}{(MC)_{min}}\left(1-\frac{(MC)_{min}}{(MC)_{max}}\right)]}{1-\frac{(MC)_{min}}{(MC)_{max}}exp[-\frac{UA}{(MC)_{min}}\left(1-\frac{(MC)_{min}}{(MC)_{max}}\right)]} \tag{3}$$

Where Q_{max} represents the maximum heat transfer capacity that a heat exchanger can potentially achieve, W; $(Mc)_{min}$ is fluid with small heat capacity, W/K; t_1', t_2' respectively represent the inlet temperatures of hot fluid and cold fluid, ℃, ε is heat exchange efficiency; UA is the heat transfer coefficient of heat exchanger, W/K.

Tab 2. Key parameters of heat exchanger

Parameter	Values	Unit

Design temperature of primary side inlet and outlet	120/45	℃
Design temperature for secondary side inlet and outlet	40/50	℃
Design flow rate for primary and secondary sides	14/103	m^3/h
Calculate pressure drop on the primary and secondary sides	1/66.8	kPa
Heat Exchange Area	43.05	m^2
Total heat transfer coefficient	1118	$W/m^2 \cdot K$
heat load	1180	kW

3.2.2 Pump Model

The water pump provides power for the hot water circulation in the heating system, and its power consumption is also an important part of the energy consumption of the heating system. In the study, a model of the water pump is established based on the performance curve and the similarity rate of the water pump. The performance curve of the water pump is shown in the Fig 8, this provide data for pump simulation.

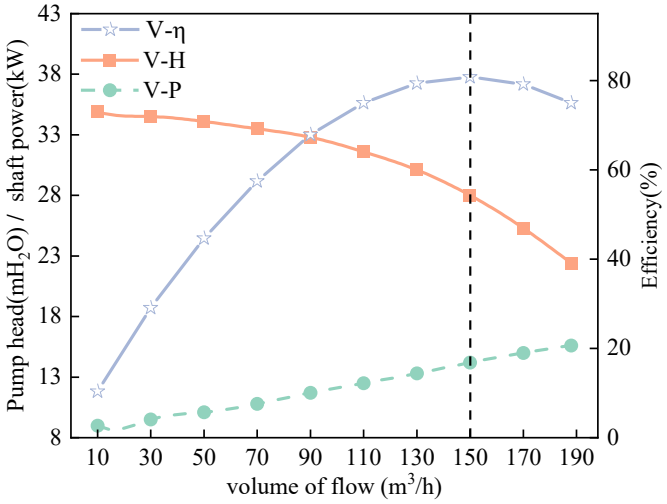

Fig 8. Pump performance curve chart

The flow work (W_{flo}) obtained by the fluid is

$$W_{flo} = V \cdot \Delta P \tag{4}$$

Where V is volume flowrate, m^3/s; ΔP is the pressure drop, Pa.

The calculation formulas for the comprehensive efficiency of the water pump (η), hydraulic efficiency (η_{hyd}), and motor efficiency (η_{mot}) are as follows:

$$\eta = \frac{W_{flo}}{P_{mot}} = \eta_{hyd}\eta_{mot} \tag{5}$$

$$\eta_{hyd} = \frac{W_{flo}}{W_{hyd}} \tag{6}$$

$$\eta_{mot} = \frac{W_{hyd}}{P_{mot}} \tag{7}$$

The head and power of other operating conditions are as follows:

$$\Delta P = r_N{}^2 \cdot s(\frac{V}{r_N}, d) \tag{8}$$

$$P = r_N{}^3 \cdot s\left(\frac{V}{r_N}, d\right) \tag{9}$$

Where W_{hyd} and P_{mot} represent the hydraulic work and motor power of pump, respectively; The term r_N denotes the speed ratio, while $s\left(\frac{V}{r_N}, d\right)$ represents a spline interpolation function, where d corresponds to the sample values under rated operating conditions. As shown in Fig 9, the relative errors of flow rate and power in the pump model are controlled within ±3%.

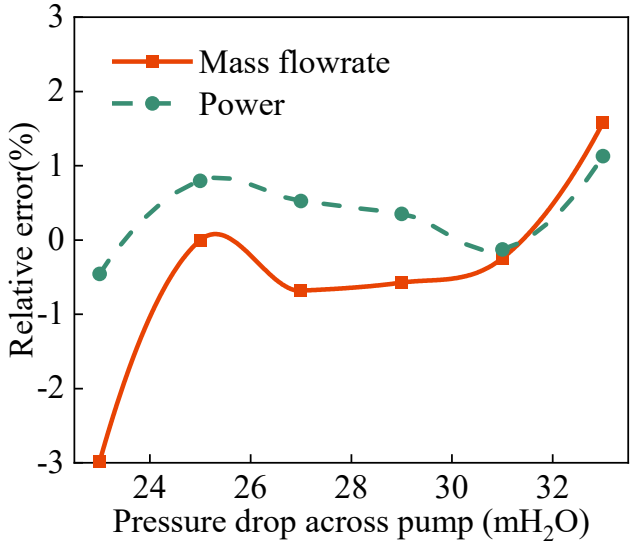

Fig 9. Flow and power of pump model

3.2.3 Pipeline flow heat transfer model

The equations for flow and heat transfer in a one-dimensional circular tube are determined by the three main flow equations, the calculation equation of the local resistance coefficient, and the comprehensive calculation equation of the thermal resistance.

$$\frac{\partial(\rho A)}{\partial t} + \frac{\partial(\rho A v)}{\partial x} = 0 \tag{10}$$

$$\frac{\partial(\rho A v)}{\partial(t)} + \frac{\partial(\rho A v^2)}{\partial x} = -A\frac{\partial p}{\partial x} - F_F - A\rho g\frac{\partial z}{\partial x} \tag{11}$$

$$\frac{\partial\rho\left(u+\frac{v^2}{2}\right)A)}{\partial t} + \frac{\partial(\rho v\left(u+\frac{p}{\rho}+\frac{v^2}{2}\right)A)}{\partial x} = -A\rho v g\frac{\partial z}{\partial x} + \frac{\partial}{\partial x}\left(kA\frac{\partial T}{\partial x}\right) + \dot{Q}_e \tag{12}$$

The resistance loss of pipeline flow is calculated by the following formula:

$$dp = \lambda\frac{l}{D}\frac{\rho v^2}{2} \tag{13}$$

$$\lambda = \frac{1.325}{(ln(\frac{\delta}{3.7D}+\frac{5.74}{Re^{0.9}}))^2} \tag{14}$$

Where v represents average velocity, m/s; p represents average pressure, Pa; T represents average temperature, ℃; ρ represents average density, kg/m^3; u represents specific internal energy,

J/kg; z represents elevation difference, m; A represents area perpendicular to the x-direction, m^2; g represents gravitational acceleration, m/s^2; l represents pipe length, m; D represents pipe diameter, m; δ represents roughness of the inner surface of the pipe, m; λ represents frictional resistance coefficient, dimensionless.

The maximum depth of frozen soil in the region is 0.43 m. The average burial depth of the pipeline is 0.82 m, and the thermal resistance of the pipeline is in the Tab 3. The temperature distribution of soil at different depths is shown in the Fig 10. The soil temperature at pipeline burial depth varies nearly linearly, and we use the average soil temperature to calculate heat loss during transport. The length and thermal resistance information for different pipe sections are shown in the attached Table B.

Tab 3. Pipeline parameter table

Nominal Diameter	External diameter x wall thickness (mm)	Insulation thickness (mm)	Thermal resistance ($m \cdot K/W$)
DN65	76×4.0	29	3.65
DN80	89×4.0	32.5	3.53
DN100	108×4.0	42.8	3.77
DN125	133×4.0	42.5	3.18
DN150	159×4.5	41.6	2.71

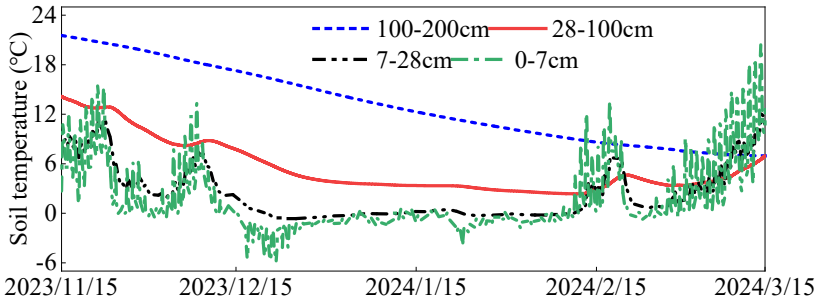

Fig 10. Soil temperature distribution map

3.2.4 Valve Model

The valve model consists of a transmission fluid interface and a valve body. The transmission fluid interface serves as a connector to transmit parameters such as fluid flow rate, pressure, enthalpy, etc. The main body determines the hydraulic characteristic equation of the valve.

$$Q_{valve} = Kv(Cv) \cdot \sqrt{\frac{dp_v}{\frac{\rho_m}{\rho_0}}} \tag{15}$$

$$\frac{Q_{valve}}{Q_{max}} = R^{(\frac{l}{l_{max}}-1)} \tag{16}$$

The term Q_{valve} represents the actual flow rate, m^3/h; dp_v denotes the pressure drop across the valve, bar; while ρ_m represents the density of the medium, kg/m^3; and ρ_0 corresponds to the density

of water at 4°C, kg/m³; Q_{max} denotes the maximum flow capacity, m³/h; R is the adjustable ratio, l indicates the valve stroke, and l_{max} corresponds to the maximum valve stroke.

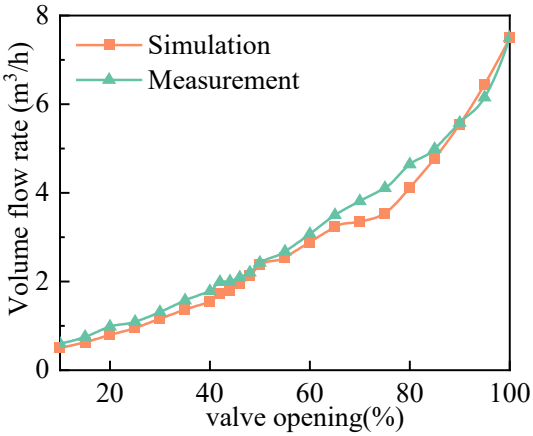

Fig 11. Comparison of valve testing and simulation results

The accuracy of the model is evaluated using MAPE and Root Mean Square Error (RMSE), and the calculation formula is as follows:

$$MAPE = \frac{1}{n}\sum_{i=1}^{n}\frac{|V_{m,i}-V_{s,i}|}{V_m} \times 100\% \quad (17)$$

$$RMSE = \sqrt{\frac{1}{n}\sum_{i=1}^{n}(V_{m,i} - V_{s,i})^2} \quad (18)$$

$V_{m,i}$, $V_{s,i}$, n represent measured values, simulated values, and sample sizes respectively.

In the study, a valve regulating model is established and validated based on the valve data measured at a pressure difference of 100 kPa (Table C). The simulation and measured results are shown in the Fig 11, The RMSE between simulation and actual measurement results is 0.25m³/h, with MAPE of 9.6%.

3.2.5 Building Model

This study selects the RC model based on a trade-off between the research objective of comparing system-level control strategies and the need for computational efficiency in large-scale simulation. The RC model, calibrated with real-world data, sufficiently captures the core thermal dynamics of buildings, thereby providing a reliable and practical simulation foundation for strategy comparison while ensuring computational feasibility.

The building model includes the indoor air and radiator heat transfer model, heat transfer between indoor and outdoor environments, and the local resistance model of the building. Based on the [34] and the European Norm EN 442-2 radiator model, a heating transfer model of the building space is established. Simplify the environmental boundary conditions in the building room temperature model, and for non-transparent enclosure structures, add the long wave radiation and short wave radiation of the sun equivalent to temperature to the dry bulb temperature of the air; for transparent enclosure structures, consider the transmitted solar radiation. The information on the building envelope structure is shown in appendix Table A. The thermal resistance information of the

building envelope structure is shown in Tab 5.

The weight factor for the v-th enclosure structure window and wall is defined as：

$$B_v = \frac{U_v A_v}{\sum_{v=1}^{p} U_v A_v} \tag{19}$$

Where B_v is weight factor; U_v, represents the heat transfer coefficient, $\mathrm{W/m^2 \cdot K}$; A_v represents the area, $\mathrm{m^2}$.

The calculation formulas for wall equivalent long wave temperature (T_{EquLw}), wall equivalent short wave temperature (T_{EquSw}), window equivalent long wave temperature ($T_{EquLwWin}$), window equivalent temperature ($T_{EqAirWin}$), and wall equivalent temperature ($T_{EqAirExt}$) are:

$$T_{EquLw} = \frac{(T_{BlaSky} - T_{DryBul}) \cdot h_{Rad}}{h_{Rad} + h_{ConWallOut}} \tag{20}$$

$$T_{EquSw} = \frac{HSol \cdot a_{Ext}}{h_{Rad} + h_{ConWallOut}} \tag{21}$$

$$T_{EquLwWin} = \frac{(T_{BlaSky} - T_{DryBul}) \cdot h_{Rad}}{h_{Rad} + h_{ConWinOut}} \tag{22}$$

$$T_{EqAirWin} = T_{DryBul} + T_{EquLwWin} \tag{23}$$

$$T_{EqAirExt} = T_{DryBul} + T_{EquLw} + T_{EquSw} \tag{24}$$

T_{BlaSky}, T_{DryBul} respectively represent Sky Black-Bulb Temperature and Dry-Bulb Air Temperature ℃; h_{Rad}, $h_{ConWallOut}$ respectively represent radiative heat transfer coefficient, convective heat transfer coefficient of exterior wall, $\mathrm{W/m^2 \cdot K}$; $HSol$ represents solar radiation, $\mathrm{W/m^2}$; a_{Ext} represents exterior wall surface absorptivity, dimensionless.

The heat exchange between the European Norm EN 442-2 radiator and the indoor environment consists of convective and radiative heat exchange. The specific calculation formula is as follows:

$$Q_{Rad,Con}{}^{i} = \frac{(T^i - T_{air})(1 - f_{Rad})UA}{N(T^i - T_{air})^n} \tag{25}$$

$$Q_{Rad,Rad}{}^{i} = \frac{(T^i - T_{rad}) f_{Rad} UA}{N(T^i - T_{rad})^n} \tag{26}$$

Where, T^i represents the temperature of the i-th discrete unit, °C; T_{air} denotes the indoor air temperature, °C; and T_{rad} signifies the radiant temperature, °C; f_{Rad} defines the radiative heat transfer fraction; while UA corresponds to the heat transfer coefficient of the radiator, W/K; Additionally, n indicates the radiator's heat transfer exponent; N gives the total number of discrete radiator units.

Based on the energy conservation principle, a thermal resistance-capacitance (RC) model of the building is developed, with its thermal network depicted in Fig 12. The equivalent temperature of windows and exterior wall surfaces is derived by superimposing the equivalent radiant temperature onto the air dry-bulb temperature. The model integrates convective and radiative heat transfer from radiators while accounting for internal heat gains. Key thermal interactions considered include:

a) Heat exchange between the building envelope's exterior surface and outdoor environment;

b) Radiative heat transfer among interior envelope surfaces;

c) Convective heat transfer between air and interior surfaces;

d) Combined convective-radiative heat transfer between air and radiators;

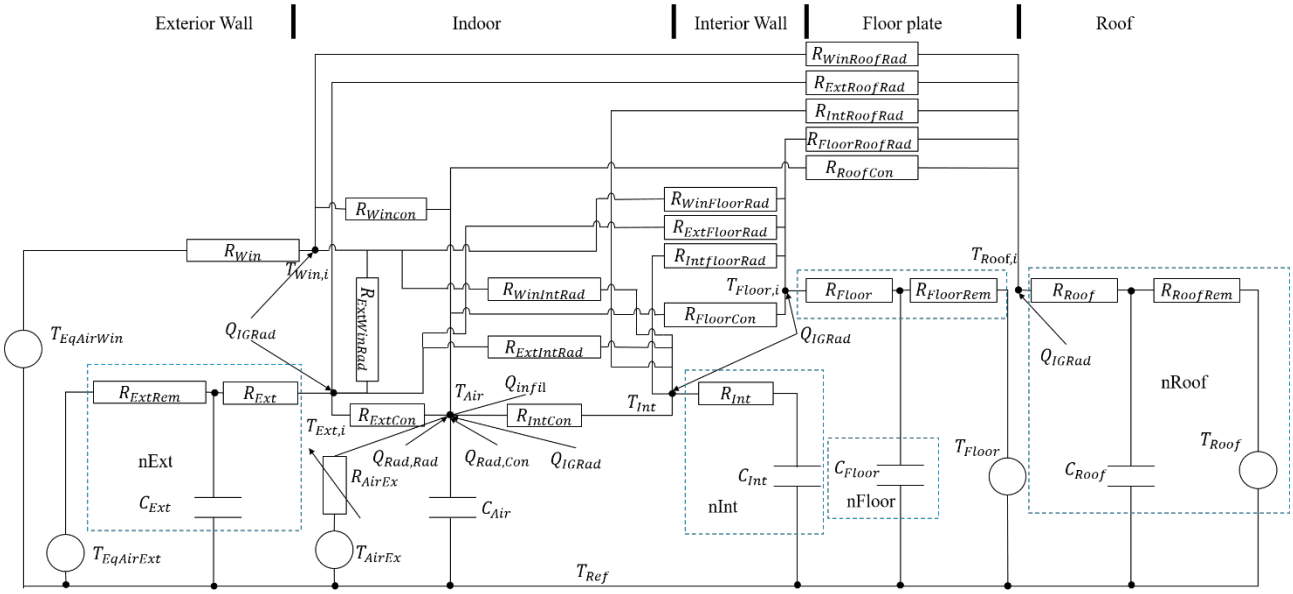

Fig 12. Schematic diagram of RC grey box model

The discrete-time state-space equations for the RC thermal network model are formulated as follows, the thermal resistance and capacitance values are provided in the Tab 5, the thermal performance parameters of the enclosure structure are shown in Appendix A.

The temperature change formulas for the exterior wall, roof, interior wall, and floor of the enclosure structure are as follows:

$$C_{Ext}\frac{dT_{Ext,i}}{dt}=\frac{T_{EqAirExt}-T_{Ext,i}}{R_{ExtRem}+R_{Ext}}+\frac{T_{Roof,i}-T_{Ext,i}}{R_{ExtRoofRad}}+\frac{T_{Floor,i}-T_{Ext,i}}{R_{ExtFloorRad}}+\frac{T_{Int}-T_{Ext,i}}{R_{ExtWinRad}}+\frac{T_{Win,i}-T_{Ext,i}}{R_{ExtWinRad}}+\frac{T_{Air}-T_{Ext,i}}{R_{ExtCon}}+Q_{IGRad}+Q_{SolRad} \quad (27)$$

$$C_{Roof}\frac{dT_{Roof}}{dt}=\frac{T_{Win,i}-T_{Roof,i}}{R_{WinRoofRad}}+\frac{T_{Ext,i}-T_{Roof,i}}{R_{ExtRoofRad}}+\frac{T_{Int}-T_{Roof,i}}{R_{IntRoofRad}}+\frac{T_{Floor,i}-T_{Roof,i}}{R_{FloorRoofRad}}+\frac{T_{Floor}-T_{Roof,i}}{R_{Roof}+R_{RoofRem}}+Q_{IGRad} \quad (28)$$

$$C_{Int}\frac{dT_{Int}}{dt}=\frac{T_{Air}-T_{Int}}{R_{IntCon}}+\frac{T_{Ext,i}-T_{Int}}{R_{ExtIntRad}}+\frac{T_{Roof,i}-T_{Int}}{R_{IntRoofRad}}+\frac{T_{Floor,i}-T_{Int}}{R_{IntFloorRad}}+\frac{T_{Win,i}-T_{Int}}{R_{WinIntRad}}+\mathrm{Q}_{IGRad} \quad (29)$$

$$C_{Floor}\frac{dT_{Floor,i}}{dt}=\frac{T_{Air}-T_{Floor,i}}{R_{FloorCon}}+\frac{T_{Floor}-T_{Floor,i}}{R_{Floor}+R_{FloorRem}}+\frac{T_{Win,i}-T_{Floor,i}}{R_{WinFloorRad}}+\frac{T_{Ext,i}-T_{Floor,i}}{R_{ExtFloorRad}}+\frac{T_{Int}-T_{Floor,i}}{R_{IntFloorRad}}+Q_{IGRad} \quad (30)$$

The formula for calculating indoor temperature is:

$$C_{Air}\frac{dT_{Air}}{dt}=\frac{T_{Ext,i}-T_{Air}}{R_{ExtCon}}+\frac{T_{AirEx}-T_{Air}}{R_{AirEx}}+\frac{T_{Int}-T_{Air}}{R_{IntCon}}+\frac{T_{Roof,i}-T_{Air}}{R_{RoofCon}}+\frac{T_{Floor,i}-T_{Air}}{R_{FloorCon}}+\frac{T_{Win,i}-T_{Air}}{R_{WinCon}}+Q_{IGRad}+\mathrm{Q}_{Rad,Rad}+Q_{Rad,Con} \quad (31)$$

$$Q_{infil}=0.278c_pV\rho_w(T_{air}-T_{DryBul}) \quad (32)$$

$T_{Ext,i}$, $T_{EqAirExt}$, $T_{Roof,i}$, $T_{Floor,i}$, T_{Int}, $T_{Win,i}$ and T_{Air} are the inner surface temperature of the exterior wall, equivalent outer surface temperature of the wall, inner surface temperature of the roof, inner surface temperature of the floor, inner surface temperature of the interior wall, inner surface temperature of the window, and indoor air temperature, respectively, ℃; C_{Ext}, C_{Air}, C_{Int}, C_{Floor}, C_{Roof} are the external wall heat capacity, air heat capacity, internal wall heat capacity, floor heat capacity, and roof heat capacity, respectively, J/K; Q_{IGRad}, $Q_{Rad,Rad}$, $\mathrm{Q}_{Rad,Con}$ are internal heat gain, radiator radiation heat exchange, radiator convective heat exchange, W; $R_{ExtRoofRad}$,

$R_{RoofCon}$, R_{Ext} the radiative thermal resistance between the inner surface of the exterior wall and the roof, the convective thermal resistance between the roof and indoor air, and the thermal resistance of the exterior wall, respectively, with units of K/W. The calculation of Q_{infil} can be seen in literature [33]. Other thermal resistance parameters follow analogous definitions, which will not be reiterated for brevity.

Tab 4. Internal heat source table

Room type	Bedroom	kitchen	Washroom	Other room
Furniture factor	30	30	30	1
Set minimum illuminance(lx)	75	100	75	75
Number of personnel(Person/m^2)	0.067	0.13	0.067	0.067
Per capita caloric intake (W)	53	60	60	60
Lighting power density(W/m^2)	15	13	15	5
Electric thermal conversion rate	0.9	0.9	0.9	0.9
Equipment power(W/m^2)	12.7	48.2	0	0

The sources of heat gain inside the building are presented in Tab 4. By considering the utilization rates of personnel, lighting, and equipment in various room types depicted in Fig 13, we calculate the internal heat gain of the building referring to literature [33].

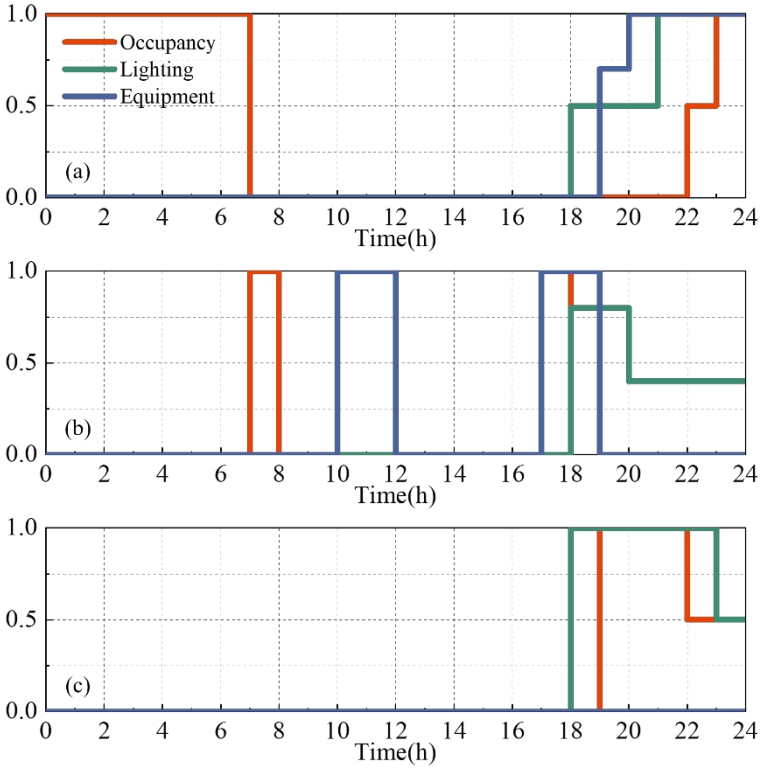

Fig 13. The occupancy rate, lighting rate, equipment rate of different room, (a) Bedroom, (b) kitchen (c) Washroom

The resistance of fluid flow inside a building is modeled as $dp_b = Sm_b{}^2$, and the coefficient S is determined by the thermal inlet flow rate and pressure drop under nominal operating conditions. Finally, we used Modelica language to build the building model as shown in the Fig 14.

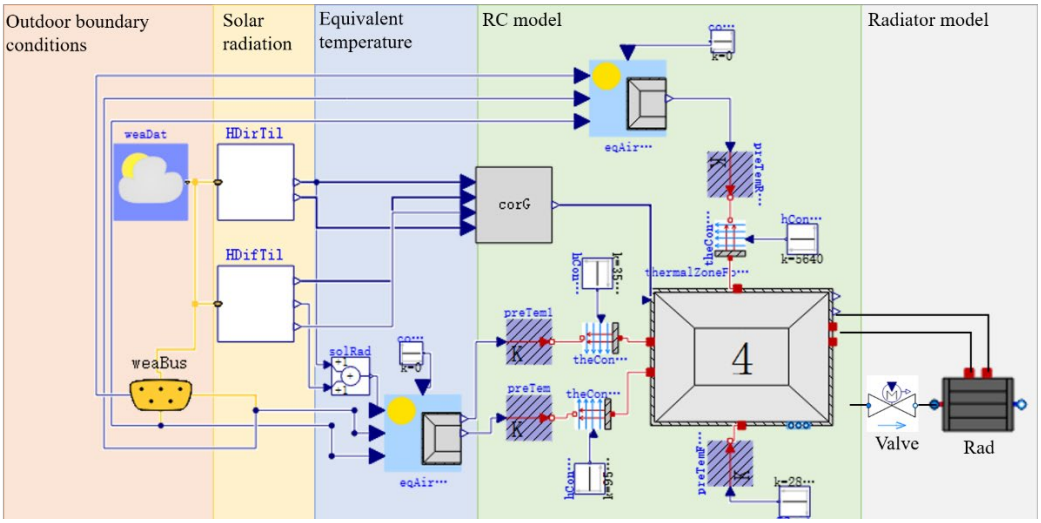

Fig 14. Building Model Component Diagram in Modelica

Tab 5. Thermal resistance and heat capacity information of enclosure structure

Building	Type of enclosure structure	Area (m^2)	Convective coefficient (W/m^2K)	Thermal resistance (K/W)	heat capacity (KJ/K)
#I type building	East wall	195	23.3/3.5	0.0198	6.3E+04
	South wall	705	23.3/3.5	0.0055	2.3E+05
	West wall	195	23.3/3.5	0.0198	6.3E+04
	North wall	705	23.3/3.5	0.0055	2.3E+05
	Interior wall	521	3.5	0.0008	1.4E+05
	Roof	240	4/1	0.0131	1.6E+05
	Floor	240	4	0.0064	1.3E+05
#II type building	East wall	198	23.3/3.5	0.0195	6.4E+04
	South wall	312	23.3/3.5	0.0124	1.0E+05
	West wall	198	23.3/3.5	0.0195	6.4E+04
	North wall	312	23.3/3.5	0.0124	1.0E+05
	Interior wall	175	3.5	0.0123	4.6E+04
	Roof	167	4/1	0.0189	1.1E+05
	Floor	167	4	0.0093	9.2E+04

The measured natural indoor temperature data over two days from the research group was compared with the simulated data, as shown in Fig 15. The RC room temperature model achieved a MAPE of 8.12%, demonstrating good accuracy. The radiator-coupled RC room temperature model was used to simulate the heating conditions from January 1 to January 7, with an initial indoor temperature of 12°C, a fixed supply water temperature of 39.1°C, and a constant flow rate of 1.05

kg/s. The resulting variations in indoor and return water temperatures are shown in Fig 16. Due to the lack of precise flow rate control, fluctuations in outdoor weather conditions influenced indoor temperature, causing it to oscillate around 20°C. While some variability was observed, the thermal load demand was met. The model effectively captured overheating effects, though the primary focus of this section was establishing the room temperature model. Further control optimization will be addressed in subsequent studies.

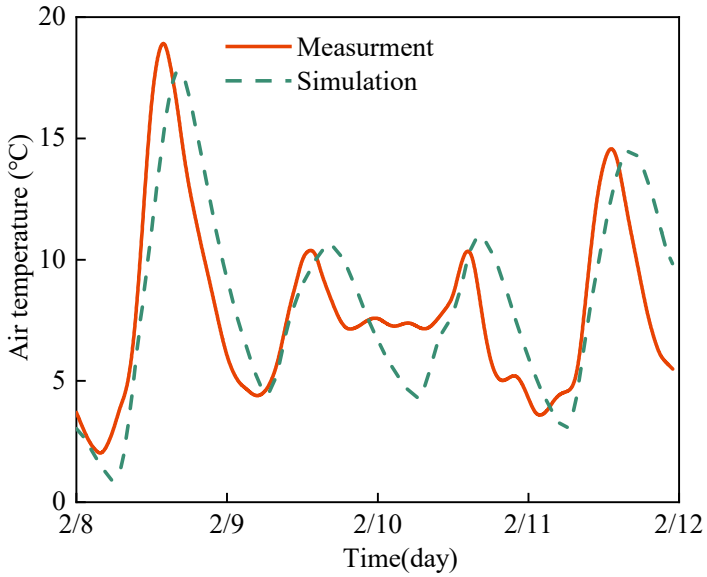

Fig 15. RC model validation

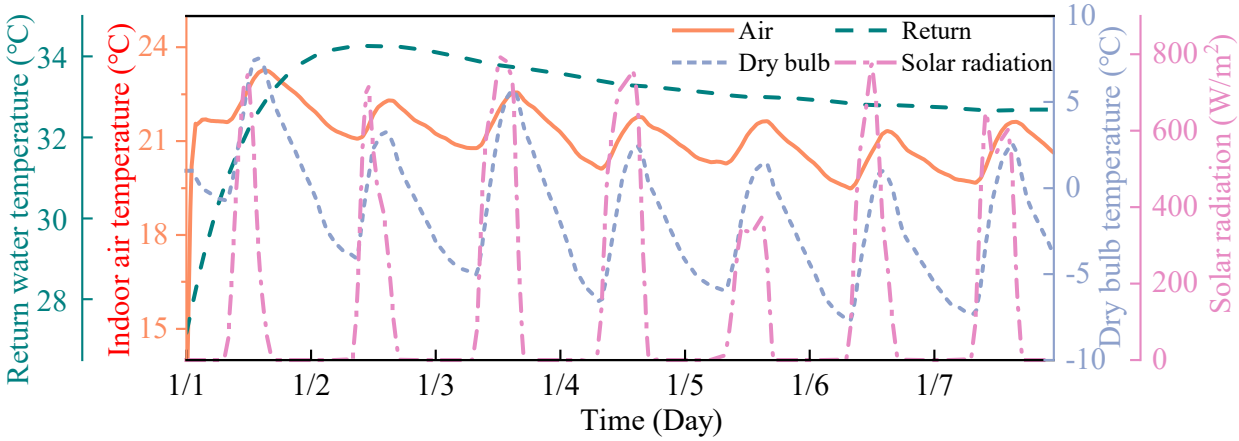

Fig 16. Response of RC model coupled with radiator model

3.3 Model Validation

This study validated the model using three indicators: the return water temperature of the heat exchange station, the supply water pressure, and the energy consumption of the water pump, the model component chart is shown in Fig 17, the results are shown in the Fig 18.The simulation model was validated using measured supply water temperature and flow rate data from January 1 to 7, demonstrating high accuracy in predicting system performance with a MAPE 5.8% for pump energy

consumption in Fig 18.(a), while thermal performance validation showed return water temperature relative errors ranging from -6.6% to 3.6% in Fig 18.(b), and hydraulic performance validation revealed heat exchanger inlet pressure relative errors between -3.2% and 6.5% in Fig 18(c), with total flow rate remaining stable throughout the validation period, the observed abrupt pressure fluctuations were likely caused by main circuit valve adjustments, collectively confirming the model's reliability for engineering analysis as all prediction errors remained within ±7% for thermal characteristics, hydraulic behavior, and energy consumption.

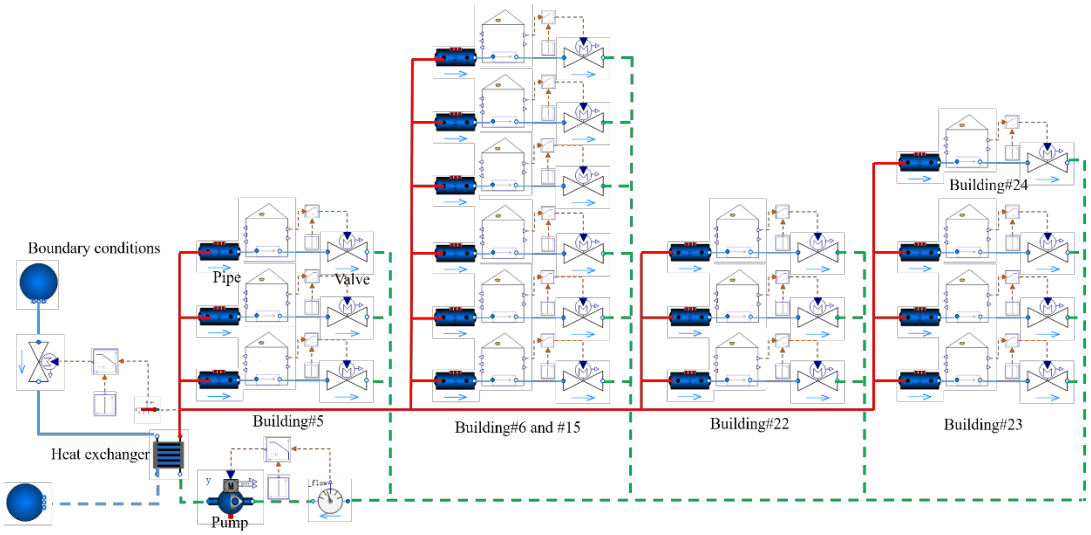

Fig 17. System simulation model diagram established using OpenModelica

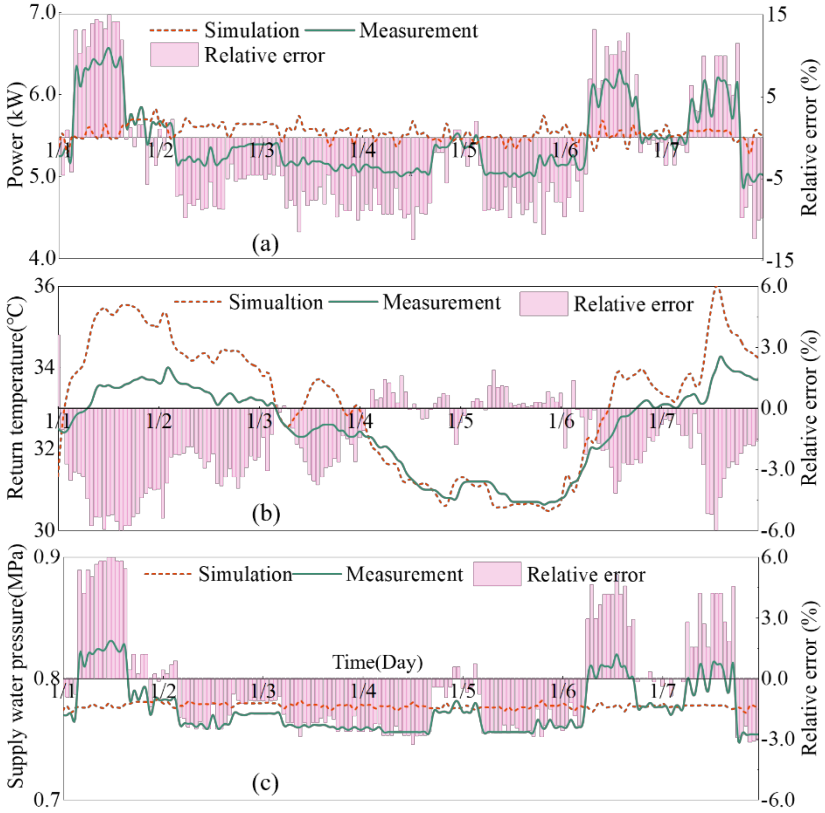

Fig 18. Model validation results. (a) Pump energy consumption, (b) Return water temperature, (c) Supply water pressure

3.4 Improvement of water supply temperature for DH station

As shown in Fig 19, the response simulation of room temperature and flow rate of a single building within 1/1 day is conducted at a fixed water supply temperature and a variable water supply temperature. A PID controller is employed, with the flow rate constrained to a range of 0.2 to 1.5 kg/s. The simulated water supply conditions are a fixed water supply temperature of 36 ℃ and a water supply temperature based on outdoor temperature. When regulating the fixed water supply temperature, setting the water supply temperature too high can easily lead to low flow conditions in order to maintain the room temperature when the outdoor temperature is high. Conversely, setting the water supply temperature too low can result in the maximum flow rate not meeting the heat load requirements when the outdoor temperature is low. The traditional heating system, which adjusts the water supply temperature curve based on the relative heat load ratio, also has similar problems due to building thermal inertia, leading to fluctuations in room temperature around the design set point.

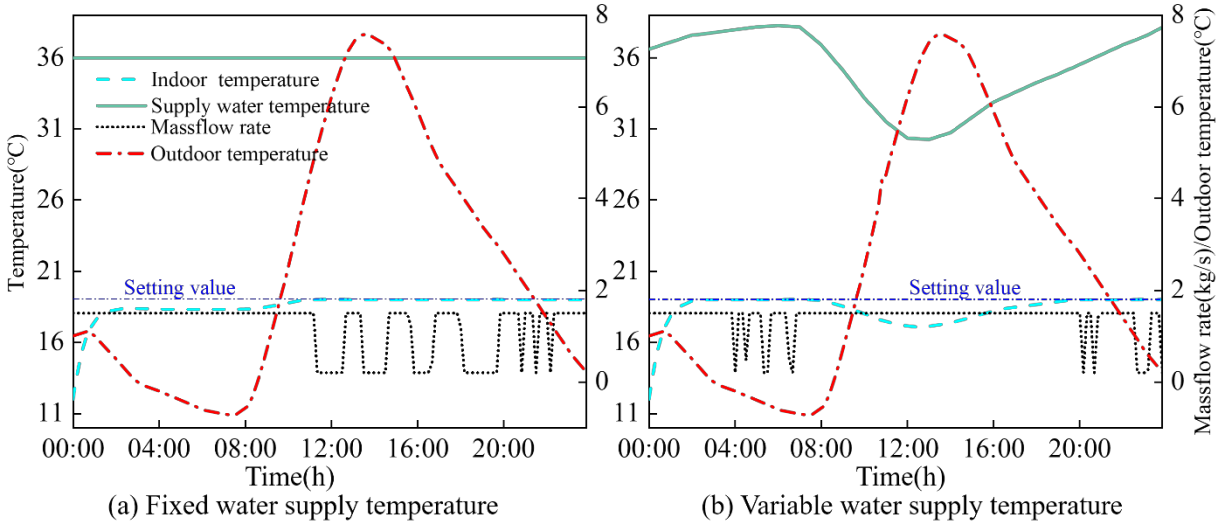

Fig 19. Room temperature response under different water supply temperature

When adjusting the thermal inlet regulating valve based on the indoor temperature feedback from the building, it is worth considering how to determine the supply water temperature of the heat exchange station. The optimal supply water temperature curve should minimize the action or range of the regulating valve while meeting the demand for end-of-pipe heating, and avoid significant hydraulic fluctuations.

Tab 6. Fitting results table

Building Type	Variable	Coefficient	95.0% confidence lower limit	95.0% confidence upper limit	R^2
Class I buildings	Intercept	-2.83	-2.97	-2.69	0.94
	Coefficient of water supply temperature	0.61	0.61	0.61	
	Coefficient of outdoor temperature	0.22	0.22	0.22	
Class II	Intercept	-2.93	-2.97	-2.89	0.97

buildings	Coefficient of water supply temperature	0.58	0.58	0.59
	Coefficient of outdoor temperature	0.30	0.30	0.30

By employing the validated room temperature RC model, the optimal water supply temperature can be inversely determined to ensure adequate heat delivery to the heat exchange station. The control valve further modulates the thermal output to maintain the predetermined indoor temperature setting point. The methodological approach involves utilizing the calibrated building-specific room temperature model to simulate heating performance under varying water supply temperatures at design flow rates. This yields room temperature variations across different heating conditions, which are subsequently fitted as a multivariate linear polynomial function of water supply temperature and outdoor temperature. Through this functional relationship, the required water supply temperature can be derived inversely for a given target room temperature. The corresponding fitting results are presented in Tab 6.

4 Results

This section summarizes the comparative performance across different control strategies, analyzing: (1) operational status of DH substations, (2) spatial distribution of room temperatures, (3) energy consumptions, and (4) potential carbon emission implications.

4.1 Operation condition

First, we provide the PID parameters used in the simulation in Tab 7 . These coefficients are determined based on engineering experience and are identical for each valve under the same control method.

Tab 7. PID parameter table for different methods

Items	SHE		RFC		FTRC	
	k_p	k_i	k_p	k_i	k_p	k_i
Pump	1	0.1	Constant frequency		5	0.1
Valve	Constant valve opening		0.1	0.1	1	0.01

4.1.1 hydraulic characteristics

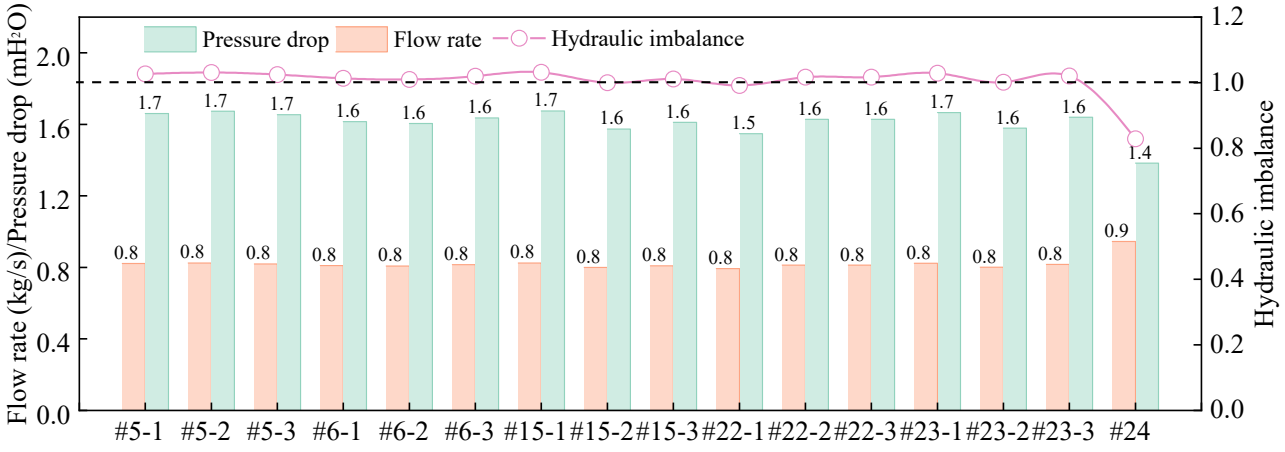

Fig 20. Hydraulic characteristics of thermal users under SHE

Under SHE, this article uses x_s to evaluate hydraulic conditions, and the calculation formula is as follows：

$$x_s = \frac{m_{actual}}{m_{design}} \tag{33}$$

x_s represents hydraulic imbalance, m_{actual}, m_{design} represent actual flow, design flow. 0.8kg/s for building type II, 1.14kg/s for building type I.

Combining Fig 25, Fig 26, Fig 20, When regulating consumer flow rates under design conditions, room temperature fluctuations of ±0.73°C persist—while meeting basic heating requirements, thermal comfort remains suboptimal. Case #24 demonstrates that even at non-design flow rates (78% of nominal values), temperatures can still fluctuate within the design range. The current SHE control methodology relies critically on precise heat load and design flow calculations, a prerequisite that proves challenging to satisfy in field implementations due to uncertainty propagation，dynamic network effects measurement limitations.

As Fig 21, under the SHE control strategy, 90% of measured return water temperatures fall below theoretical values, indicating enhanced heat transfer between air and radiators that elevates indoor air temperatures beyond set points. Consequently, implementing RTC demonstrates measurable energy savings, elucidating the thermodynamic mechanism underlying RTC's superior efficiency compared to conventional SHE methods.

Under the RTC strategy, consistent return water temperatures across thermal consumers are achieved, with the control performance demonstrated in Fig 22. When analyzed in conjunction with Fig 27, the results show that RTC maintains an average room temperature of 19.56°C significantly closer to the design value of 19.00°C compared to SHE (20.47℃) operation.

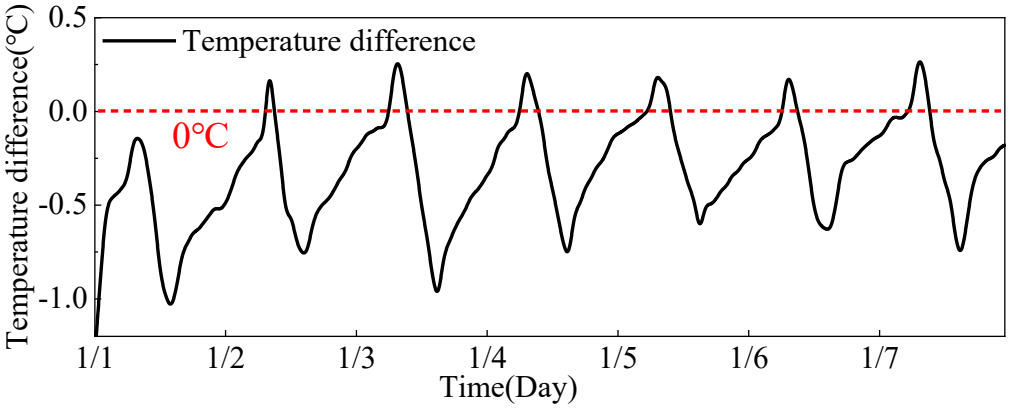

Fig 21. Temperature difference of return water temperature between theoretical and actual under SHE

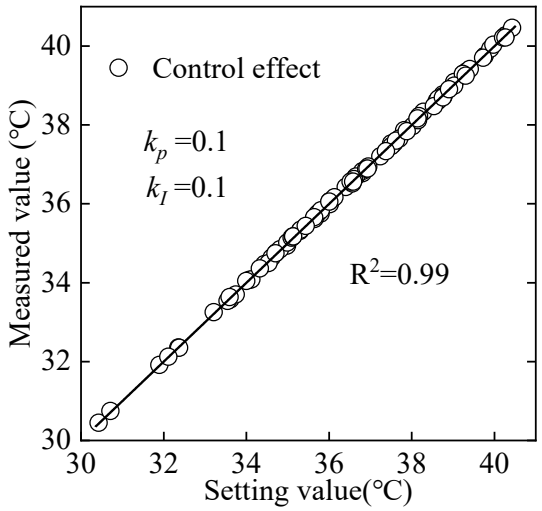

Fig 22. Return water temperature control effect under RTC

Fig 23 demonstrates distinct valve operation characteristics between RTC and RTFC control strategies. RTC maintains relatively stable valve openings (#24: 61.2±2.9%; #5-1: 32.0±3.0%), while RTFC exhibits significantly larger variations (#24: 32.8±12.5%; #5-1: 34.0±10.9%) to achieve tighter room temperature control (±0.1°C). Under RTFC, the flow rates of most heat users fluctuate below the design flow rate, which tends to be set on the higher side. In contrast, under RTC, user flow rates fluctuate around the design flow rate, resulting in stronger hydraulic stability compared to RTFC.The observed differences stem from RTFC's more responsive control algorithm, highlighting an inherent compromise between control precision and valve operation stability in district heating systems.

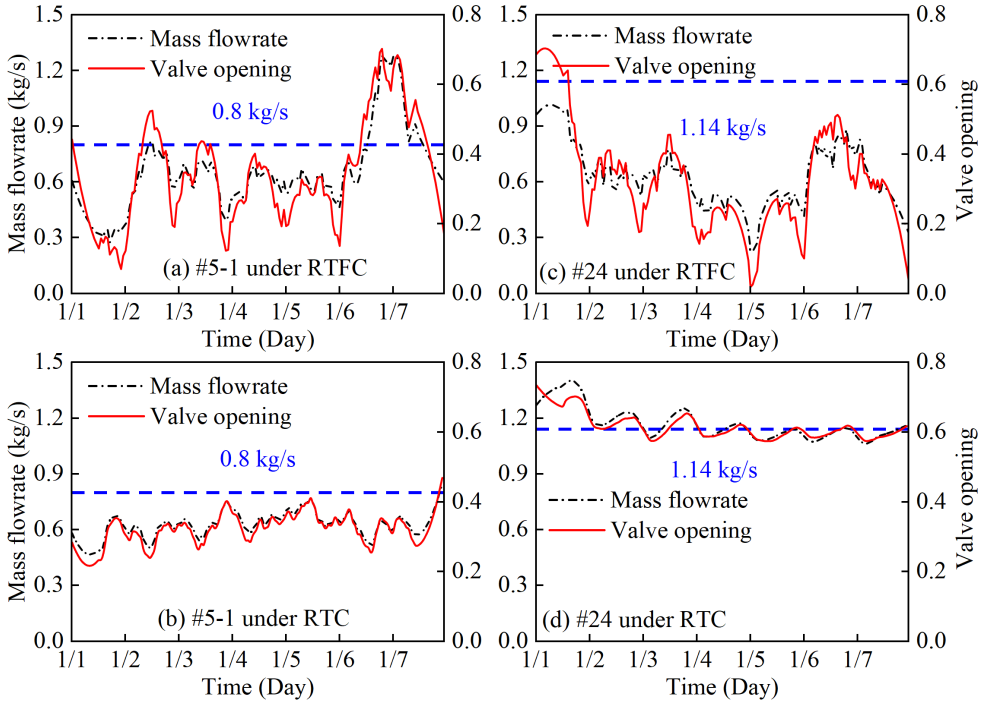

Fig 23. Hydraulic characteristic under RTC and RTFC

4.1.2 Compare between RTFC and actual

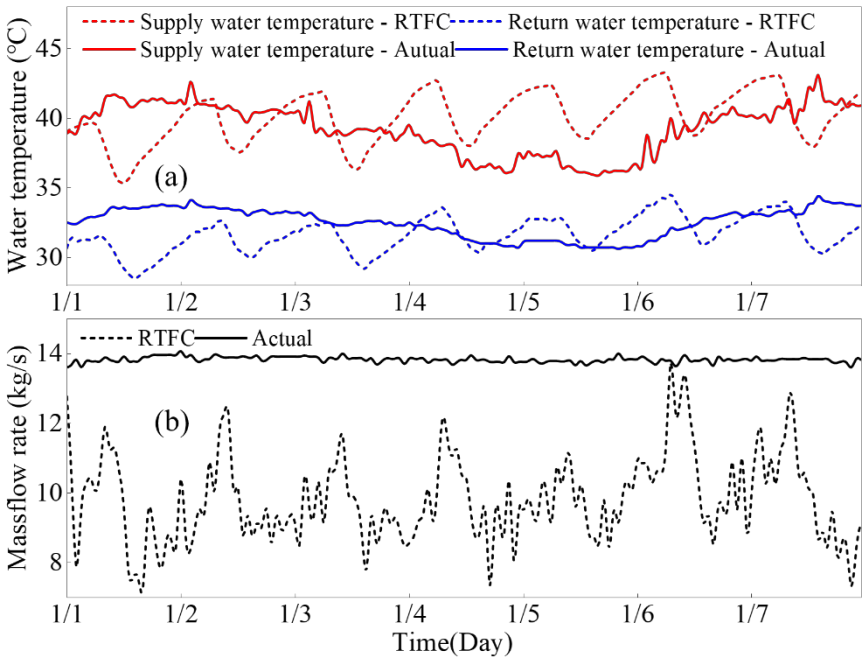

Fig 24. Comparison of operating parameters between RTFC and actual, (a) Supply and return water temperature, (b) Mass flowrate

As in Fig 24.(a), the RTFC method demonstrates significant improvements in thermal regulation performance through dynamic adjustments of supply water parameters, exhibiting a higher frequency of supply temperature changes compared to conventional operation that effectively maintains room temperature stability within ±0.1°C of the set point. Besides, the RTFC improved thermal transfer

efficiency as evidenced by the elevated supply-return temperature difference (8.45°C versus 6.75°C). The 1.7°C (25.2%) increase in temperature difference indicates enhanced heat extraction from the distribution system. As in Fig 24.(b), hydraulic analysis shows that while conventional operation maintained a constant mass flowrate of 13.82 kg/s (SD=0.08), the RTFC implemented coordinated flow rate modulation between 7.28~13.72 kg/s with supply temperature variations, achieving a 34.3% average flow reduction. With these operational modifications collectively contributing to a 15.98% reduction in pumping energy while maintaining equivalent thermal comfort conditions, thereby validating the effectiveness of RTFC in optimizing district heating system performance.

4.2 Room temperature distribution

Room temperature stability is critically important for ensuring thermal comfort, energy efficiency, and system reliability in heating systems. Excessive fluctuations not only compromise occupant well-being—particularly for vulnerable groups—but also lead to increased energy consumption and accelerated equipment wear. By implementing feedback control, temperature variations can be reduced by over 90%, as demonstrated in our case study, thereby optimizing operational efficiency, extending system lifespan, and supporting carbon neutrality goals through lower emissions. This underscores the necessity of advanced regulation in modern HVAC and DHS.

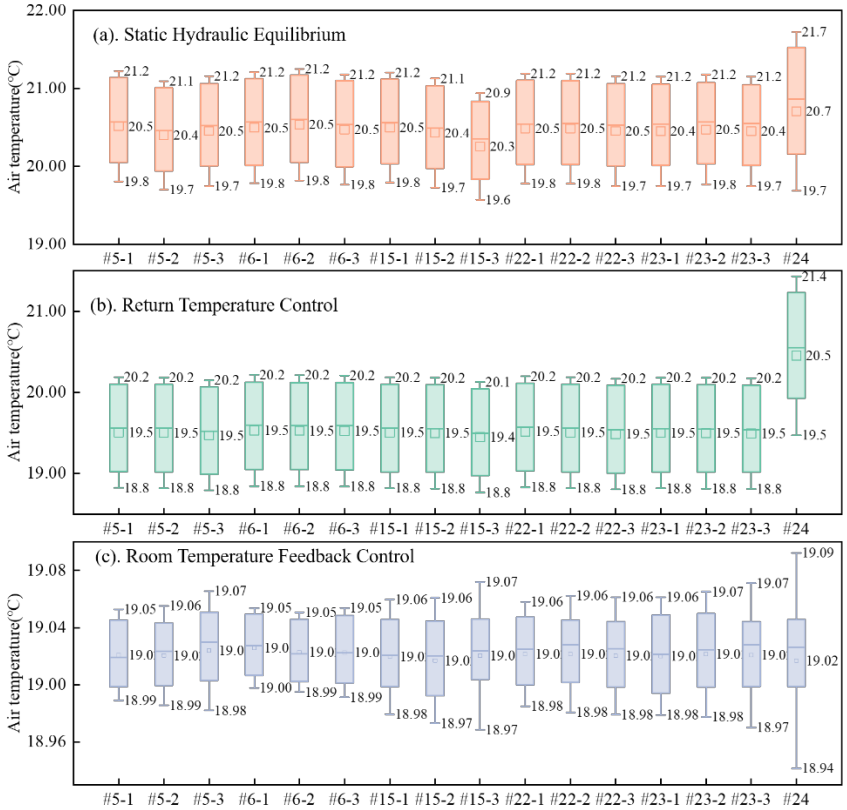

Fig 25. Comparison of room temperature distribution, (a) SHE, (b)RTC, (c) RTFC

As shown in Fig 25, Fig 26, under SHE, the average room temperature exceeded the design setting point of 19°C, with significant fluctuations observed among individual users. The standard

deviations of room temperature for the two user categories were 1.02°C and 0.70°C. Respectively, when applying the RTC, the mean room temperature aligned more closely with the design value of 19°C, the corresponding standard deviations for the two user groups were 0.98°C and 0.68°C, representing marginal improvements over static balance regulation. In contrast, RTFC demonstrated superior stability, restricting temperature fluctuations to within ±0.1°C. The observed standard deviations decreased substantially to 0.24°C and 0.12°C for the respective user categories, achieving 75% and 83% reductions compared to static regulation. This confirms the efficacy of feedback control in ensuring thermal stability.

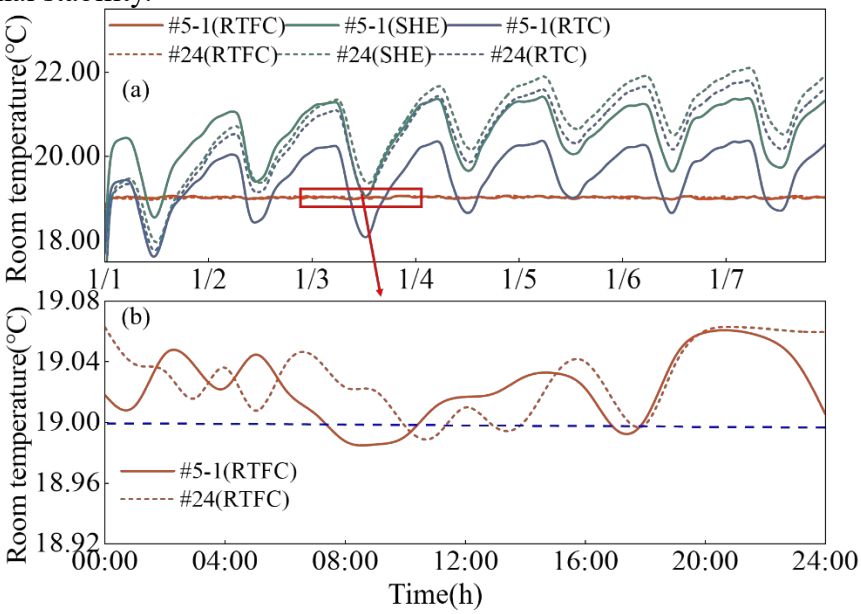

Fig 26. Details of room temperature changes, (a) Under different control strategies, (b) A day of RTFC

In the Fig 27, SHE does not implement dynamic flow control during system operation. RTC indirectly regulates flow by adjusting the return water temperature, thereby gradually bringing the indoor temperature closer to the design value. However, both regulation methods exhibit limited effectiveness in reducing the dispersion of indoor temperature distribution and fail to significantly improve temperature uniformity. In contrast, RTFC demonstrates superior performance. This regulation method not only more effectively meets the required indoor design temperature but also significantly enhances thermal stability. Simulation results show that when room temperature feedback control is applied, the standard deviation of indoor temperature decreases from 1.54°C to 0.04°C, a reduction of 97.4%, indicating a substantial improvement in temperature control precision. Notably, under actual operating conditions, the fluctuation amplitude of indoor temperature still exhibits considerable deviation, suggesting that the system retains significant potential for optimization in temperature control strategies.

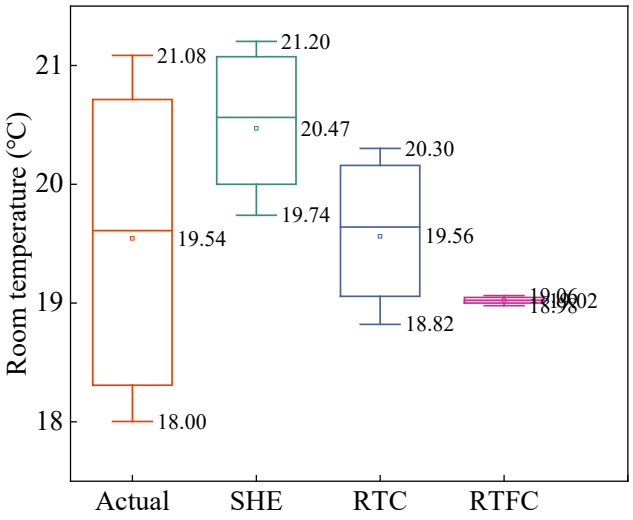

Fig 27. Comparison of total room temperature distribution

As shown in Fig 28, for actual conditions, the mean room temperatures for thermal users #24 and #5-1 were 19.86°C and 19.58°C, with standard deviations of 0.67°C and 1.07°C. Respectively, after implementing room temperature feedback control, the mean temperatures stabilized at 19.00°C and 19.02°C, while the standard deviations significantly decreased to 0.25°C and 0.08°C, representing reductions of 62.7% and 92.5%, respectively. This demonstrates a substantial improvement in temperature stability.

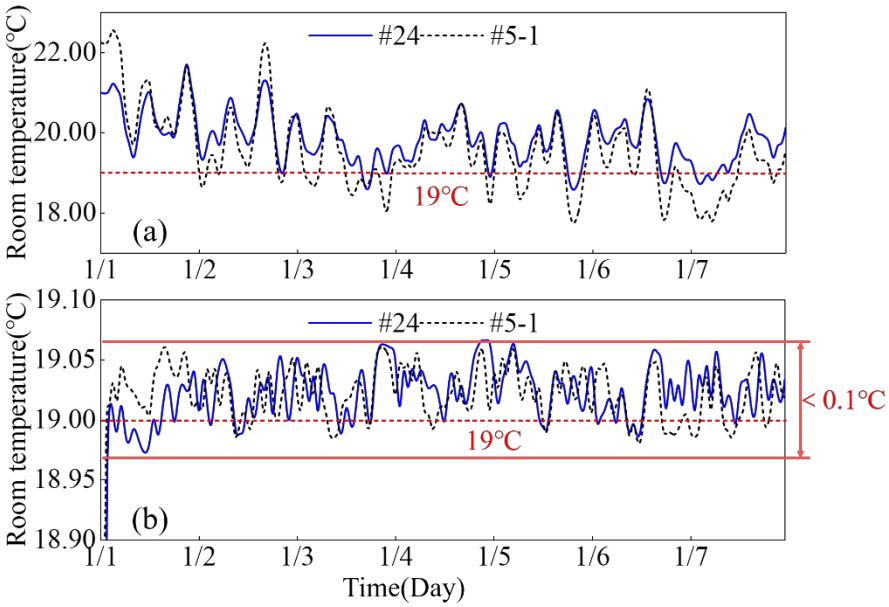

Fig 28. Comparative of room temperature, (a) Under actual of #24 and #5-1, (b) Under RTFC of #24 and #5-1

4.3 Energy consumptions

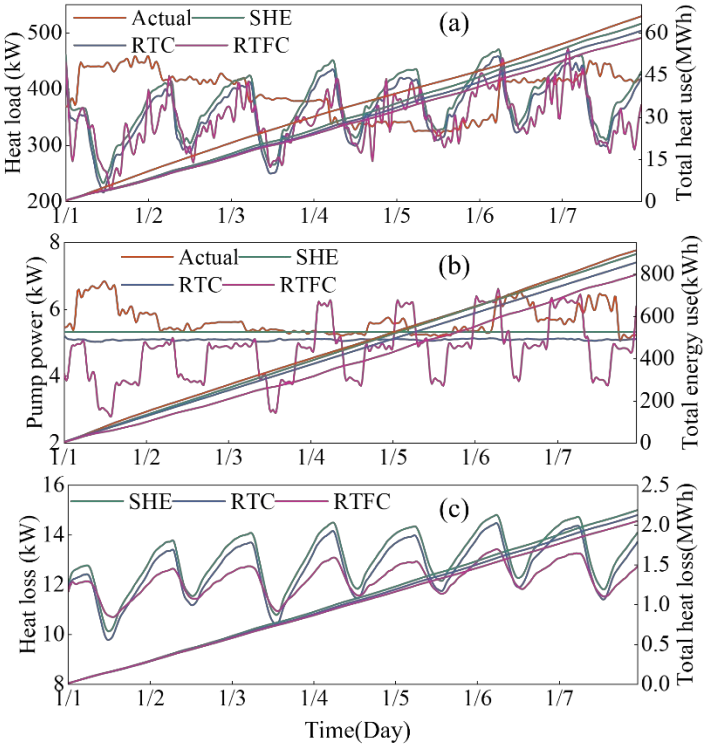

Fig 29. Energy use under three control methods, (a) heat consumption, (b) electricity consumption, (c) heat loss

The heat consumption, power consumption, and heat loss under the three control modes are shown in the Fig 29. The heat consumption and electricity consumption under the three regulation strategies are as Tab 8.

Tab 8. Energy Consumption Comparative Statistics

Energy use	Actual (Bsee line)	SHE	RTC	RTFC
Heat consumption (kWh)	65825	63207	60719	58138
Electricity consumption (kWh)	951	895	856	799
Reduction of heat consumption	-	3.98	7.76	11.68
Reduction of electricity consumption	-	5.89	9.99	15.98

Compared to the Actual case, the SHE strategy reduces heat and electricity consumption by 3.98% and 5.89%, respectively. The RTC strategy achieves equivalent reductions in heat (3.98%) and slightly higher savings in electricity (9.99%). The proposed RTFC strategy delivers the most significant overall savings, reducing heat consumption by 11.68% and electricity consumption by 15.98%.

The energy savings achieved by RTC primarily stem from regulating the return water temperature, which marginally reduces indoor temperature fluctuations. In contrast, RTFC delivers energy savings through variable-frequency pump control and optimized supply water temperature at the heat exchange station. Furthermore, RTFC significantly diminishes indoor temperature variations,

thereby enhancing thermal comfort.

4.4 Potential for carbon reduction through technology promotion

Based on the energy-saving rate indicators and collected energy consumption data obtained in this study, this section evaluates the energy-saving and emission-reduction potential of the precise control technology at different regional levels. Using 2022 as the baseline year, the case study data were obtained from actual measurements by a heating company, while the regional heating totals were sourced from statistical yearbooks (excluding steam heating). Electricity consumption data were converted using the power transmission and distribution ratio (55.5). The carbon emission factors for electricity and heat are 0.9350 tCO_2/MWh and 94.4 tCO_2/TJ, respectively.

The results demonstrate that this technology can achieve significant carbon emission reductions across all evaluated levels—including the case study community, the case heating system, Huanghua City, Cangzhou City, and Hebei Province (Fig 30 for details). If implemented across Hebei Province's 1.19 billion m² heating area, the technology could reduce CO_2 emissions by at least 4 million tons annually, with a per-unit area reduction of 3.49 kg CO_2/m². The case study location exhibits low urban energy efficiency, suggesting greater emission reduction potential upon wider implementation of this technology.

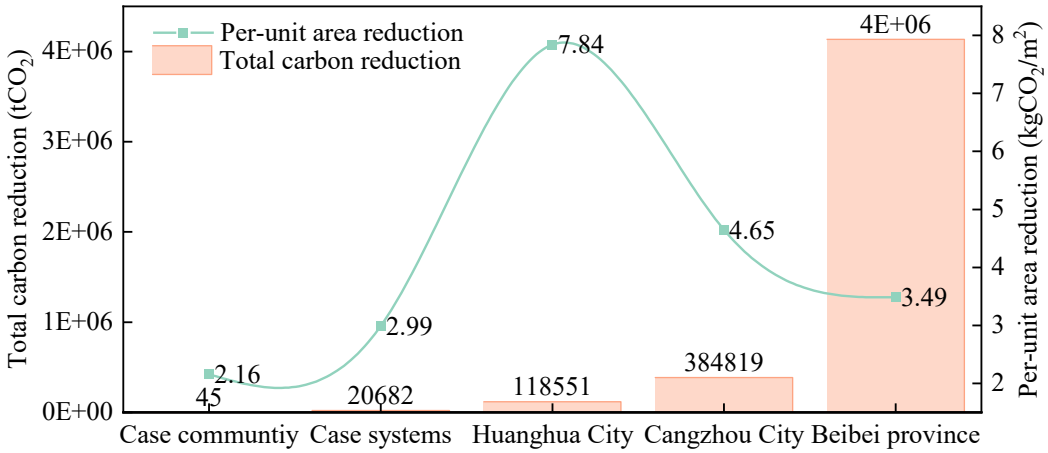

Fig 30. Quantitative analysis of carbon emission reductions in different level

4.5 Dynamic Economic Analysis

The benefits following the installation of the control valve primarily stem from reduced heat and electricity consumption. The resulting fuel cost savings are calculated based on the average efficiency of the coal-fired hot water boiler as the heat source. Given that the average thermal efficiency of coal-fired boilers typically ranges from 70% to 85%, a value of 77.5% is applied for this calculation, alongside an average calorific value of 12 MJ/kg for lignite coal. As the water pump operates continuously throughout the heating season, the associated electricity cost savings are computed using the average electricity price.

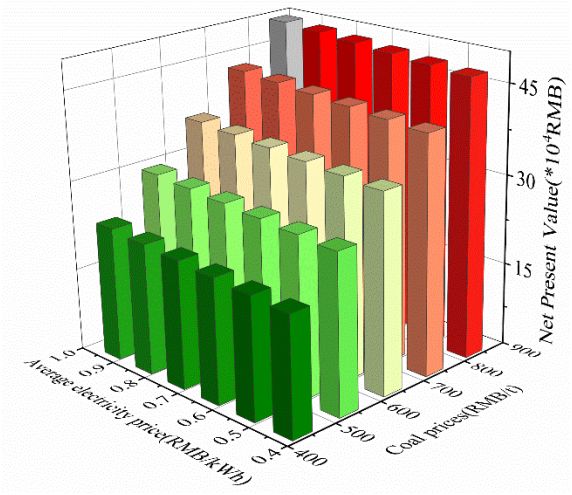

Fig 31. The impact of coal and electricity prices on net present value

As shown in Fig 31, the net present value (NPV) is significantly more susceptible to coal price than to electricity price. Specifically, a 100 RMB/t rise in coal price boosts the NPV by 67,000 RMB, which is substantially greater than the 5,200 RMB increase resulting from a 0.1 RMB/kWh rise in electricity price.

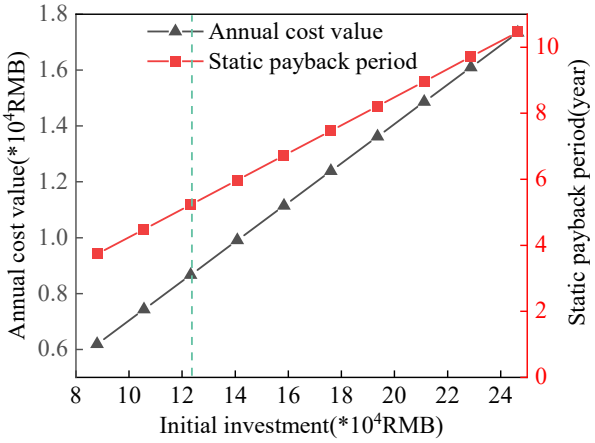

Fig 32. The impact of initial investment changes on annual cost and static payback period

Fig 32 shows the variations of both the Annual Cost and Static Investment Payback Period with the initial equipment investment. Even if the initial investment were to double, the resulting payback period would still be significantly shorter than the equipment's design life, demonstrating the project's resilient cost-recovery capability and its underlying economic viability.

5 Discussion

This study establishes a high-fidelity model encompassing the complete DHS from substations to building terminals, with comprehensive validation of multivariate system parameters. Building upon this foundation, we propose and implement RTFC control for thermodynamic inlet valves, establishing a multi-level control framework that coordinates DH stations, circulating pumps, and

thermodynamic inlet valves. This integrated approach achieves significant reduction of indoor temperature fluctuations and enhanced system-wide energy efficiency. The novel direct-room-temperature control paradigm fundamentally circumvents the thermal imbalance issues inherent in conventional hydraulic-balance-based methods, maintaining precise thermal regulation within ±0.1°C deviation. Notably, this represents the first demonstration of building-terminal-oriented control that simultaneously addresses both hydraulic and thermodynamic performance in operational DH systems.

The proposed RTFC demonstrates superior thermal stability and energy efficiency compared to state-of-the-art approaches. Specifically:

Thermal Stability: While prior studies (Literature [11] & [12]) achieved temperature fluctuations of ±0.30°C and ±0.35°C respectively, RTFC establishes a significant advancement with unprecedented precision (±0.1°C), representing a 67-71% improvement in stability.

Energy Efficiency: RTFC outperforms conventional methods with 11.68% thermal energy savings and 15.98% electrical energy reduction, substantially exceeding Literature [11] (6.1%) and [12] (7.4%). Although Literature [35] reported comparable thermal savings (12%), its temperature control precision (>±0.1°C) remains inferior to the sub-degree stability demonstrated herein.

While Literature[33] demonstrated building-level zonal control for individual building, this study advances the field through district heating (DHS) system-wide regulation. Building upon these complementary approaches, future research should focus on developing an integrated control framework that combines building-scale zoning with network-level optimization to achieve comprehensive thermal distribution management across entire DHS networks. However, the hydraulic influence of substation primary-side valve regulation remains insufficiently characterized, particularly regarding its propagation effects through interconnected network loops and consequent impacts on overall system stability.

The demonstrated performance breakthrough stems from RTFC's novel integration of three key technological components: (i) direct room-temperature tracking that fundamentally eliminates the hydraulic-thermal decoupling prevalent in conventional systems, (ii) a multi-level cooperative control architecture enabling system-wide coordination, and (iii) real-time adaptive regulation simultaneously implemented at both substation and terminal levels.

Although the specific numerical results vary by case, the findings of this study, together with existing literature, consistently indicate that feedback control strategies directly targeting end-user thermal comfort (such as RTFC) can, in principle, unlock greater energy-saving potential and better avoid over- or under-supply compared to conventional control strategies.

The method for determining the supply water temperature explicitly incorporates indoor temperature as a key factor. Since indoor temperature variations are primarily driven by meteorological conditions, as well as the thermal characteristics of the building envelope and radiator performance, the derived water temperature model is, therefore, applicable to regions with similar climates.

The primary objective of PID tuning is to ensure the tracking stability and rapidity of the system under its respective set points. Under the premise of meeting basic stability, we observe that fine adjustments to PID parameters can affect the absolute energy consumption values, but they do not alter the relative trends or conclusions of the energy consumption comparison across different strategies.

It should be noted that while RTFC's instantaneous flow fluctuations for temperature stability raise hydraulic concerns in large networks, its fundamental benefit lies in reducing average and peak flows, thereby lowering overall network load and pumping energy. A balance between control and stability could be achieved by algorithmic flow-rate constraints and more responsive pressure controls. This study validates RTFC's subsystem-level efficiency; its large-scale hydraulic dynamics warrant further investigation.

6 Conclusion

This study proposes a RTFC control method for thermal entrance regulation, demonstrating adaptable compatibility with diverse terminal-equipped DH substations. The developed methodology effectively addresses two persistent challenges: excessive building temperature fluctuations and high energy consumption at DH substations. Specifically, RTFC incorporates an innovative supply water temperature determination algorithm to prevent drastic valve opening adjustments at thermal entrances, thereby ensuring hydraulic network stability. Key findings from the implemented case study include:

(1) Modeling pipeline flow dynamics based on governing flow equations eliminates the need for empirical resistance testing and identification procedures, while integrating RC building thermal models into DHS simulations enables coupled hydraulic-thermal performance analysis.

(2) The SHE approach adequately meets basic thermal demands while exhibiting room temperature fluctuations of ±0.73℃. In comparison, RTC demonstrates superior energy efficiency with approximately 4% energy savings relative to SHE. However, comparative analysis reveals that RTC does not demonstrate superior capability in reducing room temperature fluctuations relative to SHE. While they maintain comparable implementation feasibility in existing district heating systems.

(3) The proposed methodology introduces a novel supply temperature determination algorithm for DH substations to ensure guaranteed heating capacity. When integrated with variable-speed pump operation, the RTFC strategy reduces room temperature fluctuations from ±1.07°C to within ±0.1°C，representing a significant advancement in thermal stability assurance for modern DHS.

(4) The implementation of RTFC demonstrates significant efficiency improvements compared to conventional DHS operation, achieving an 11.68% reduction in thermal energy consumption, a 15.98% decrease in electrical energy use, and 2.16 $kgCO_2/m^2$ lower carbon emissions, with provincial-scale projections for Hebei Province indicating potential emission reductions exceeding 3.49 $kgCO_2/m^2$.

7 Acknowledgments

This work was supported by the China National Key Research and Development Program - China-Finland intergovernmental cooperation in science and technology innovation (2021YFE0116200), and NSFC-RS international exchange projects: Digital-twin based smart control of low-carbon heating under climate change (NSFC funding No.52311530087 and RS funding NO. 223541).

8 Author contributions

Anqing Wang: Methodology, Writing–original draft. Haichao Wang: Conceptualization, Writing–review and editing, Funding acquisition. Tianyu Wang: Validation and Visualization. Muyan Li: Validation and Visualization. Zhiwen Luo: Supervision. Risto Lahdelma: Supervision

9 References

[1] IEA (2020), Key World Energy Statistics 2020, IEA, Paris. https://www.iea.org/reports/key-world-energy-statistics-2020

[2] Nejat P, Jomehzadeh F, Taheri MM, et al. A global review of energy consumption, CO2 emissions and policy in the residential sector (with an overview of the top ten CO2 emitting countries). RENEW SUST ENERG REV. 2015;43:843-862. https://doi.org/10.1016/j.rser.2014.11.066

[3] Lin J, Lin B. The actual heating energy conservation in China: Evidence and policy implications. ENERG BUILDINGS. 2019;190:195-201. https://doi.org/10.1016/j.enbuild.2019.03.004

[4] Zhang L, Ma X, Wang Y, et al. The increasing district heating energy consumption of the building sector in China: Decomposition and decoupling analysis. J CLEAN PROD. 2020; 271:122696. https://doi.org/10.1016/j.jclepro.2020.122696

[5] Benazeraf D, Dulac J, Collier U, et al. District Energy Systems in china options for Optimization and Diversification. 2017.

[6] T.U.B. Energy, Annual report on China building energy efficiency, China Construction Industry Publishing House, Beijing, 2023.

[7] T.U.B. Energy, Annual report on China building energy efficiency, China Construction Industry Publishing House, Beijing, 2019.

[8] D K, H T, J Y L. Empirical analysis of the demand-based heat supply system in district heating buildings. Applied Thermal Engineering, 277(2025),127031, https://doi.org/10.1016/j.applthermaleng.2025.127031.

[9] Yuan J, Wang C, Zhou Z, Study on refined control and prediction model of district heating station based on support vector machine, Energy, 189 (2019), 116193, https://doi.org/10.1016/j.energy.2019.116193.

[10] Zhang Y, Xia J, Fang H, et al, Field tests on the operational energy consumption of Chinese district heating systems and evaluation of typical associated problems, Energy and Buildings 224 (2020), 110269, https://doi.org/ 10.1016/j.enbuild.2020.110269.
[11] Li Z, Liu J, Yang X, et al, Novel effective room temperature-based predictive feedback control method for large-scale district heating substation. Applied Thermal Engineering, 218(2023), 119241, https://doi.org/10.1016/j.applthermaleng.2022.119241.
[12] Li Z, Liu J, Jia L, Improving room temperature stability and operation efficiency using a model predictive control method for a district heating station, Energy and buildings, 287(2023), 112990, https://doi.org/10.1016/j.enbuild.2023.112990.
[13] M. Dahlblom, B. Nordquist, L. Jensen, Evaluation of a feedback control method for hydronic heating systems based on indoor temperature measurements, Energy and Buildings 166 (2018) 23–34, https://doi.org/10.1016/j.enbuild.2018.01.013.
[14] G. Liu, X. Zhou, J. Yan, G. Yan, A temperature and time-sharing dynamic control approach for space heating of buildings in district heating system, Energy 221 (2021), 119835, https://doi.org/10.1016/j.energy.2021.119835.
[15] Liao Z, Swainson M, Dexter A, On the control of heating systems in the UK, Building and Environment, 40 (2005) 343–351, https://doi.org/10.1016/j. buildenv.2004.05.014.
[16] Ji Y, Chen X, Yang X, Wang X, et al, Research on the framework and meteorological parameter optimization method of dynamic heating load prediction model for heat-excha nge stations, Energy, 309(2024), 0360-5442, https://doi.org/10.1016/j.energy.2024.133125.
[17] Guelpa E, Marincioni L, Martina C, Thermal load prediction in district heating systems, Energy, 176(2019), 693-703, https://doi.org/10.1016/j.energy.2019.04.021.
[18] Liu Q, Hou H, Zhou Z, et al, A novel heat load forecasting method based on CASDA -driven unsupervised clustering, Journal of Building Engineering, 111(2025),113457, http s://doi.org/10.1016/j.jobe.2025.113457.
[19] Yao Y, Shekhar D K, State of the art review on model predictive control (MPC) in Heating Ventilation and Air-conditioning (HVAC) field, Building and Environment, 200(2021), 107952, https://doi.org/10.1016/j.buildenv.2021.107952.
[20] Zhao A J, Dong F, Xue X, et al, Optimal control for hydraulic balance of secondary n etwork in district heating system under distributed architecture, Energy and Buildings, 2 90(2023), 113030, https://doi.org/10.1016/j.enbuild.2023.113030.
[21] Chicherin S, Zhuikov A, Junussova L, The new method for hydraulic calculations of a district heating (DH) network, Energy 60(2022), 125071, https://doi.org/ 10.1016/j.energy. 2022.125071.
[22] Hakan I T, Development of a physical hydraulic modelling tool for District Heating systems, Energy and Buildings,253(2021), 111512, https://doi.org/10.1016/j.enbuild.2021.111512.
[23] Guo C, Zhang J, Yuan H, Yuan Y G, et al, Informer-based model predictive control fra mework considering group controlled hydraulic balance model to improve the precision

of client heat load control in district heating system, Applied Energy, 373(2024), 123951, https://doi.org/10.1016/j.apenergy.2024.123951.
[24] Che Z, Sun J, Na H, et al, A novel method for intelligent heating: On-demand optimized regulation of hydraulic balance for secondary networks, Energy, 282(2023), 128900, https://doi.org/10.1016/j.energy.2023.128900.
[25] Gang Su, Yongheng Peng, Wanxiang Yao, et al, Distributed control strategy of central heating system based on multi-agent consensus. Applied Thermal Engineering, 2025(262), 125136. https://doi.org/10.1016/j.applthermaleng.2024.125136.
[26] Anjun Zhao, Feifei Dong, Xiao Xue, et al, Optimal control for hydraulic balance of secondary network in district heating system under distributed architecture, Energy and Buildings, 2023 (290), 113030, https://doi.org/10.1016/j.enbuild.2023.113030.
[27] Ahmed N. Abdalla, Rendong Ji, Omar I. et al, Distributed control and optimization in building energy systems: a technical survey of multi-agent architectures and algorithms, Energy and Buildings, 2026 (350), 116644, https://doi.org/10.1016/j.enbuild.2025.116644.
[28] Rui Jing, Meng Wang, Zhihui Zhang, et al, Distributed or centralized? Designing district-level urban energy systems by a hierarchical approach considering demand uncertainties, Applied Energy, 2019 (252), 113424, https://doi.org/10.1016/j.apenergy.2019.113424.
[29] Verbeke S, Audenaert A, Thermal inertia in buildings: A review of impacts across climate and building use, Renewable and Sustainable Energy Reviews, 82(2018), Part 3, Pages 2300-2318, https://doi.org/10.1016/j.rser.2017.08.083.
[30] G.M. Soret, P. Vacca, J. Tignard, et al, Thermal inertia as an integrative parameter for building performance, Journal of Building Engineering, 33(2021), 101623, https://doi.org/10.1016/j.jobe.2020.101623.
[31] Yuan J, Huang K, Han Z, Zhou Z, et al, A new feedback predictive model for improving the operation efficiency of heating station based on indoor temperature, Energy 222 (2021), 119961, https://doi.org/10.1016/j.energy.2021.119961.
[32] Hou J, Li H, Nord N, Nonlinear model predictive control for the space heating system of a university building in Norway, Energy 253 (2022), 124157, https:// doi.org/10.1016/j.energy.2022.124157.
[33] Wang H C, Bo S, Zhu C Z, et al, A zoned group control of indoor temperature based on MPC for a space heating building, Energy Conversion and Management, 290(2023), 117196, https://doi.org/10.1016/j.enconman.2023.117196.
[34] V.D. Ingenieure, Calculation of transient thermal response of rooms and buildings - Modelling of rooms (VDI 6007).
[35] Li Z W, Liu J, Zhang J, Wang Y M, et al, A hybrid control method for district heating substations based on time-based room temperature demand, Energy and Buildings, 297(2023), 113467, https://doi.org/10.1016/j.enbuild.2023.113467.

10 Appendix

Table A. Building envelope structure information

Enclosure structure	Layers	Thickness (mm)	Density (kg/m^3)	Specific heat capacity (J/(kg•K))	Thermal conductivity (w/(m•K))	Heat transfer coefficient ($w/(m^2•K)$)
External wall	Polymer anti cracking mortar	5	0.93	1800	1050	0.249
	Polystyrene insulation board	100	0.037	50	1380	
	Cement mortar leveling layer	20	0.93	1800	1050	
	Aerated concrete block removal	200	0.18	1800	316	
	cement mortar	20	0.93	1800	1050	
Interior wall	cement mortar	20	0.93	1800	837	1.515
	Ceram site concrete	180	0.465	1200	837	
	cement mortar	20	0.93	1800	837	
Roof (top to bottom)	Extruded polystyrene Board	20	0.033	29	1791	1.105
	reinforced concrete structure	120	1.74	2500	920	
Floor	cement mortar	30	0.93	1800	837	0.645
	reinforced concrete structure	130	1.628	2500	837	
	Quartz sand	300	0.209	930	837	
Roof	reinforced concrete structure	180	1.74	2500	920	0.277
	B1 grade polystyrene board	140	0.046	19	2517	
Window	Low-e coated glass	6	0.76	2500	840	2.1
	Air	9	0.026	1.2	1006	
	Low-e coated glass	6	0.76	2500	840	
	The solar heat gain coefficient is 0.426, the shading coefficient is 0.490, the solar transmittance is 33%, the solar reflectance is 26%, the visible light transmittance is 40%, and the visible light reflectance is 23%					/

Table B. Pipeline parameter table

Number	Length (m)	Diameter (mm)	Thermal resistance (W/K)	Notes
1	107	DN100	28.44	#5 Main circuit
2	8	DN80	2.22	#5 Loop branch line
3	40	DN65	11.04	#5 Loop branch line
4	7	DN150	2.69	#6#15 Main circuit
5	17	DN125	5.36	#6#15 Main circuit
6	13	DN125	4.14	#6#15 Main circuit
7	84	DN100	22.23	#6#15 Main circuit
8	13	DN80	3.71	#6#15 Loop branch line
9	66	DN65	17.97	#6#15 Loop branch line
10	110	DN150	36.8	#22#23#24 Main circuit
11	12	DN100	3.3	#22 Main circuit
12	28	DN80	7.98	#22 Loop branch line
13	21	DN65	5.61	#22 Loop branch line
14	58	DN125	20.62	#23#24 Main circuit
15	25	DN125	7.87	#23#24 Loop branch line
16	7	DN100	1.85	#23#24 Loop branch line
17	17	DN100	4.55	#23#24 Loop branch line
18	97	DN80	27.57	#24 Main circuit

Table C. Valve characteristic measurement data at 100kPa

Valve opening (%)	Pressure drop across valve (kPa)	Measured flow (m^3/h)	Simulated flow (m^3/h)	Relative error (%)
10	100.34	0.60	0.50	15.84
15	100.34	0.75	0.63	15.96
20	99.75	0.98	0.79	19.25
25	99.69	1.09	0.95	12.83
30	99.63	1.31	1.16	11.62
35	99.86	1.57	1.37	12.99
40	99.62	1.78	1.54	13.57
42	99.83	1.99	1.71	13.83
44	100.48	2.00	1.81	9.70
46	100.34	2.09	1.96	6.11
48	99.61	2.20	2.13	3.01
50	100.23	2.42	2.37	2.03
55	99.80	2.67	2.54	4.77
60	100.40	3.07	2.89	5.92
65	100.21	3.50	3.23	7.62
70	100.28	3.81	3.35	12.15
75	100.06	4.11	3.54	13.88
80	100.20	4.64	4.11	11.39
85	100.04	4.99	4.78	4.29
90	99.75	5.58	5.55	0.58
95	100.45	6.15	6.44	-4.78
100	99.68	7.50	7.49	0.13

11 Nomenclature

Abbreviation	
DHS	District Heating Systems
DH	District Heating
SHE	Static hydraulic equilibrium
RTC	Return water temperature control
RTFC	Room temperature feedback control
MAPE	Meat absolute percent error
RMSE	Root mean square error
HVAC	Heating Ventilation and Air Conditioning
Symbols	
Q_{max}	Maximum heat transfer capacity, W
Mc	Heat capacity, W/K
t_1'	Inlet temperature of hot fluid
t_2'	Inlet temperature of cold fluid
ε	Heat exchange efficiency
UA	Heat transfer coefficient, W/K
W_{flo}	Flow work of fluid, W
ΔP	Pressure difference across water pump, Pa
η	Comprehensive efficiency
η_{hyd}	Hydraulic efficiency
η_{mot}	Motor efficiency
r_N	Speed ratio
v	Average velocity, m/s
p	Pressure, Pa
T	Temperature, ℃
ρ	Density, kg/m^3
u	Specific internal energy, J/kg
g	Gravitational acceleration, m/s^2
l	Length, m
D	Diameter, m
δ	Roughness of the inner surface of the pipe, m
λ	Frictional resistance coefficient
A	Area, m^2
Q_{valve}	Flow rate of valve, m^3/h
dp_v	Pressure drop across the valve
Kv	Flow coefficient, USG/minute, International standard

Cv	Flow coefficient, m^3/h, European and American standards
$V_{m,i}$	Measured values
$V_{s,i}$	Simulated values
f_{Rad}	Radiative heat transfer fraction
R	Heat resistance
C	Heat capacity
C_{Ext}	Heat capacity of exterior wall
$T_{Ext,i}$	Inner surface temperature of the exterior wall, ℃
$T_{win.i}$	Inner surface temperature of the window, ℃
$T_{Floor,i}$	Inner surface temperature of the floor, ℃
$T_{Roof,i}$	Inner surface temperature of the roof, ℃
Q_{IGRad}	Radiation of inter heat gain, W
Q_{SolRd}	Solar radiation, W
m_{actual}	Actual flow
m_{actual}	Design flow
Subscript	
min	Minimum value
max	Maximum value
EquLw	Equivalent long wave
EquSw	Equivalent short wave
EquLWin	Window equivalent long wave temperature
EqAirWin	Window equivalent temperature
Drybul	Dry bulb
Rad	Radiation
Con	Convection
Ext	Exterior wall

1